2023-08-31

First Order Dynamic Sliding Mode Control of a Wind Turbine with Optimized Tip Speed Ratio

Padmanabhuni, Nishanth

UNIVERSITY OF CALGARY

First Order Dynamic Sliding Mode Control of a Wind Turbine with Optimized Tip Speed Ratio

by

Nishanth Padmanabhuni

A THESIS

SUBMITTED TO THE FACULTY OF GRADUATE STUDIES

IN PARTIAL FULFILMENT OF THE REQUIREMENTS FOR THE

DEGREE OF MASTER OF SCIENCE

GRADUATE PROGRAM IN MECHANICAL ENGINEERING

CALGARY, ALBERTA

AUGUST, 2023

Abstract

This thesis explores a novel sliding mode control method to boost power from wind turbines, focusing on the power optimization region. The controller, designed for a 3rd-order system with generator torque input and rotor torque disturbance, is tested using a simple wind turbine model and FAST for validation. The first objective is to identify the optimal tip-speed-ratio (TSR) for maximum power using the Recursive Least Squares (RLS) method. The RLS generates a polynomial connecting the TSR and power coefficient, defining the wind turbine's operating point. A forgetting factor is incorporated in the RLS method for system adaptability to changing conditions. The other objective utilizes a first-order dynamic sliding mode controller with integration (FODSMCI) to control the wind turbine, keeping it at the optimal TSR for maximum power without chattering. The study revealed the RLS's effectiveness in determining optimal TSR on wind turbine models. The FODSMCI enables a balance between controller performance and rotor speed tracking, yielding a chatter-free response.

Acknowledgements

I extend my deepest gratitude to Dr. Pieper, whose guidance, expertise, and financial counsel have been indispensable in my research journey.

My sincere thanks go to my parents, for their unfaltering support and encouragement, and my friends, whose companionship and positive energy have made this process all the more enjoyable.

Thank you all for your unwavering belief in me and your invaluable contributions to my journey

Table of Contents

List of Tables

List of Figures

List of Abbreviations

Acronym		Definition
WECS	……...	Wind Energy Conversion System
HAWT	……...	Horizontal Axis Wind Turbine
VAWT	……...	Vertical Axis Wind Turbine
DFIG	……...	Doubly Fed Induction Generator
MPPT	……...	Maximum Power Point Tracking
BEM	……...	Blade Element Method
TSR	……...	Tip Speed Ratio
P&O	……...	Perturb and Observe
INC	……...	Incremental Conductance
HC	……...	Hill Climbing
MPC	……...	Model Predictive Control
PID	……...	Proportional Integral Derivative
LQR	……...	Linear Quadratic Regulator
FLC	……...	Fuzzy Logic Control
SMC	……...	Sliding mode control
RLS	……...	Recursive Least Square
FODSMCI	……...	First Order Dynamic Sliding Mode Control with Integration
ARE	……...	Algebraic Riccati Equation
MSD	……...	Mass-Spring-Damper
RMSE	……...	Root Mean Square Error
SWT	……...	Simple Wind turbine
FAST	……...	Fatigue, Aerodynamics, Structures, and Turbulence
NREL	……...	National Renewable Energy Laboratory
TurbSim	……...	Turbulence Simulator

Chapter 1 Introduction

This thesis introduces a novel sliding mode control approach for controlling wind turbines, which aims to improve their efficiency and performance. In addition, this thesis presents the development of a novel reference tracker that determines the optimal tip speed ratio for the wind turbine.

As the world confronts the challenges of climate change, resource depletion, and an increasing global demand for energy, the importance of renewable energy has become paramount. Renewable energy, derived from natural resources that are constantly replenished, such as sunlight, wind, water, and geothermal heat, offers a sustainable, clean, and virtually inexhaustible supply of energy. This has the potential to transform the way we power our lives, significantly reduce our reliance on fossil fuels, and mitigate the effects of climate change.

Fossil fuels, although still widely used, are increasingly recognized as unsustainable in the long term due to their contributions to environmental problems such as land degradation, water pollution, and greenhouse gas emissions. These issues have exacerbated the frequency of natural disasters like wildfires, hurricanes, and floods. In response, many governments, including Canada, have pledged to achieve net-zero emissions by 2050 [1] to reverse these changes and secure a sustainable future.

Among the various forms of renewable energy, wind power has emerged as a crucial player in the transition to a more sustainable energy future, harnessing the natural power of wind currents to generate electricity through the use of turbines. Advances in technology and design have led to the development of larger, more efficient turbines, capable of capturing energy at greater heights and across a wider range of wind speeds. As a result, wind energy has become one of the fastest-growing and most cost-effective renewable energy sources worldwide world [2], with countries such as the United States, China, and Germany leading the way in deployment. This showcases the potential for wind energy to provide a significant share of clean electricity for both developed and developing nations, with the possibility of providing at least 20% of global electricity production by 2050 [3].

Wind energy has emerged as the second largest source of sustainable energy and continues to grow in worldwide capacity each year. The main benefits of wind energy include the fact that the wind itself is free and sustainable, and that it doesn't pollute the air like power plants that rely on the combustion of fossil fuels. As a rapidly growing method of electrical generation, wind power is integral to the ongoing shift towards a greener global energy landscape.

1.1 Wind Energy Conversion System

Wind energy conversion systems (WECS), such as wind turbines, have gained popularity in recent years as a means to generate electricity by harnessing the kinetic energy of the wind. This form of renewable energy has several advantages, one of which is the widespread availability of wind across the globe. Historically, wind has been utilized for various purposes, including mechanical power and transportation.

When compared to other forms of energy generation, such as hydroelectric dams and solar panels, wind turbines generally have a lower environmental impact. Hydroelectric dams can cause significant disruptions to ecosystems and alter natural water flows, while the production and disposal of solar panels can contribute to environmental issues due to the materials used in their creation[4].

However, there are some drawbacks associated with wind energy conversion systems. These include the intermittency of wind speeds, which can result in unreliable power generation. Additionally, wind turbines can have noise and visual impacts on the surrounding landscape. Wildlife, particularly birds and bats, can also be at risk from collisions with the turbine blades, although the overall impact is significantly less than that of buildings, power lines, and cats combined.

Despite these challenges, wind energy conversion systems are poised to play a pivotal role in the global transition towards a more sustainable future. As advances in technology continue and investments in renewable energy infrastructure grow, wind energy has the potential to become a major player in satisfying our electricity needs. By reducing our reliance on fossil fuels and lowering our carbon footprint, wind energy can contribute significantly to a greener, cleaner world.

There are two primary categories of Wind Energy Conversion Systems – Horizontal Axis Wind Turbines (HAWTs) and Vertical Axis Wind Turbines (VAWTs) as shown in Figure 1.1 below. Although VAWTs possess certain advantages, such as ease of maintenance and adaptability to urban environments, HAWTs are frequently regarded as superior for various reasons. One of the most notable benefits of HAWTs is their heightened efficiency, attributable to their aerodynamic design, which allows them to capture and convert a greater amount of wind energy into electricity. Moreover, HAWTs are better suited for large-scale power generation projects, as they can be scaled up more effectively than VAWTs. Due to these factors, HAWTs are predominantly employed within the wind energy industry. For the purposes of this thesis, the HAWT will be discussed.

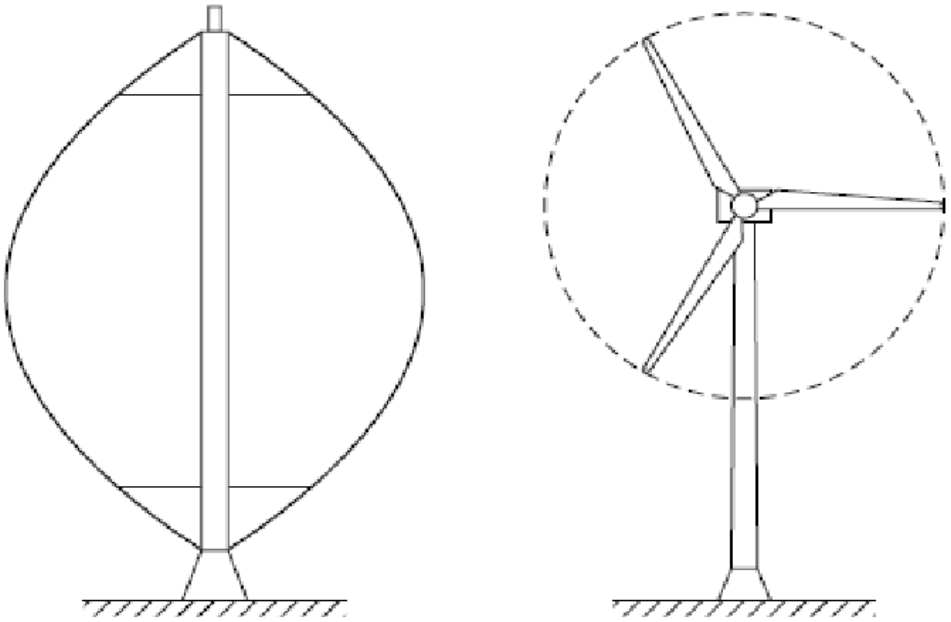

Figure 1.1 Vertical (left) and Horizontal (right) axis wind turbines *[5]*

1.2 Basic Wind Turbine System

Wind turbines play a crucial role in renewable energy generation, converting the kinetic energy of the wind into electricity. They capture the wind's energy using blades designed for efficient energy capture as the wind flows over them. These blades, mounted on a shaft, are turned by the wind, which causes the generator to rotate and produce electricity. This electricity is then sent to a transformer and distributed through power lines. Among the various wind turbine designs, the most common is the three-bladed HAWT.

Modern wind turbines consist of several key components [6]: the rotor, which includes the blades and supporting hub; the drive train, encompassing the rotating parts of the wind turbine and typically comprising a gearbox, coupling, mechanical brake, and generator; the nacelle and main frame, housing the wind turbine, bedplate, and yaw system; the tower and foundation; machine controls; and the balance of the electrical system, such as cables, switchgear, transformers, and potentially electronic power converters.

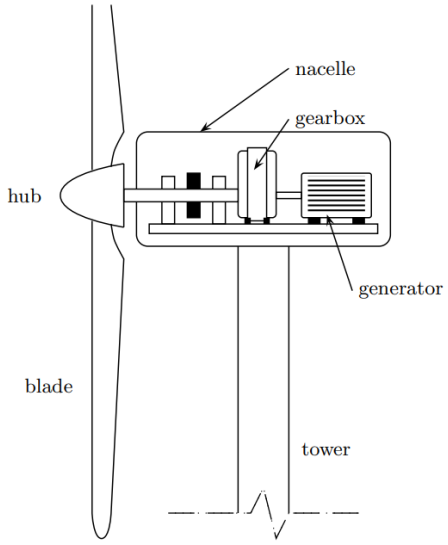

Figure 1.2 Wind Energy conversion system with horizontal axis wind turbine *[7]*

The process of wind energy capture by the blades involves the following steps: as the wind blows, it causes the rotor to turn, which subsequently rotates the shaft. The wind passing through the blades creates a pressure difference between the bottom and top surfaces of the blades, generating lift and drag forces as shown in Figure 1.3 below. As the lift-to-drag force ratio increases, the torque acting on the blade also rises, leading to the spinning of the rotor [8].

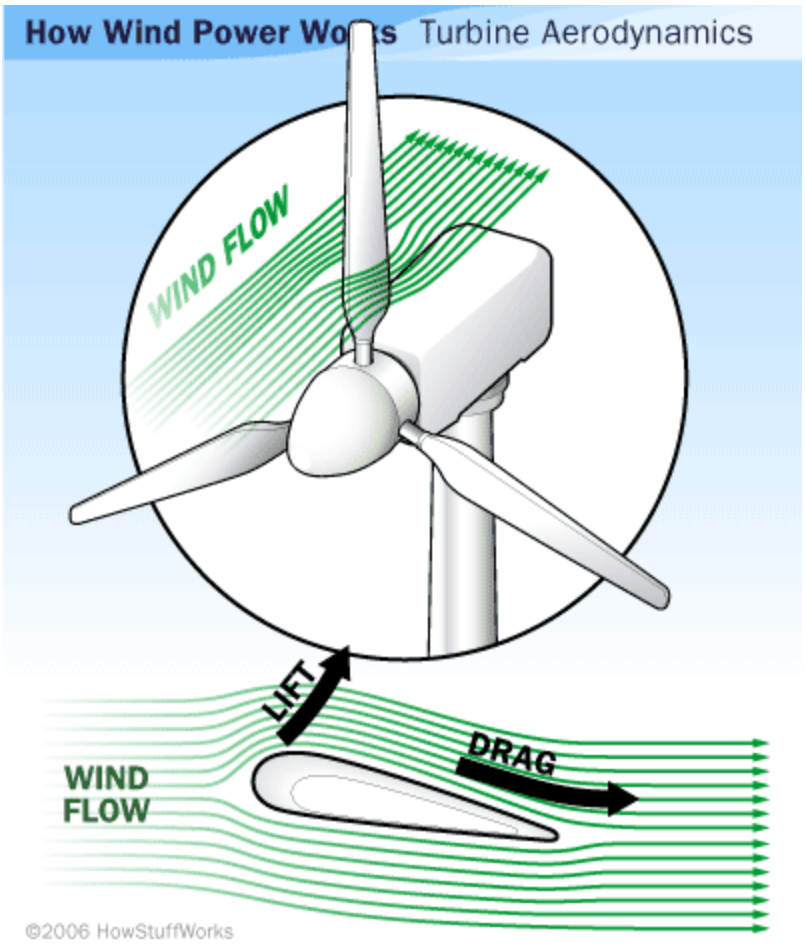

Figure 1.3 Lift and drag acting on the turbine blade *[9]*

These turbines are typically situated in areas with high wind speeds, such as on hills or offshore, to ensure maximum energy production. The energy produced by wind turbines is a renewable resource and does not emit harmful pollutants into the environment, making it a sustainable and eco-friendly source of electricity. With the continued development and advancement of wind turbine technology, wind power is set to become an increasingly important component of the world's energy mix.

As for the control system of a wind turbine, it is essential to ensure optimal machine operation and power production. A wind turbine control system encompasses various components, including sensors for speed, position, flow, temperature, current, and voltage; controllers, such as mechanical mechanisms and electrical circuits; power amplifiers, like switches, electrical amplifiers, hydraulic pumps, and valves; actuators, comprising motors,

pistons, magnets, and solenoids; and intelligence elements, including computers and microprocessors.

1.3 Control Inputs for Wind Turbines

Effective control of wind turbines is essential for optimal performance and longevity. The most common methods to control the wind turbine is pitch control and yaw control as shown in Figure 1.4. Additionally, if the generator is capable of varying its torque, it can adjust its output power to match the reference speed, which is the ideal rotational speed for maximum energy capture based on the wind turbine's design.

The first and easiest method to implement is Yaw control. It plays a crucial role in managing the rotor speed of a wind turbine. The yaw system is responsible for adjusting the orientation of the rotor to align it with the incoming wind, enabling the blades to capture the maximum amount of energy. The yaw system can be controlled using wind direction sensors and an actuator that rotates the nacelle to align it with the wind.

Pitch control involves adjusting the angle between the blade chord and the plane of rotation. By altering the pitch angle, the turbine can control the angle of attack of the blades and, consequently, the amount of lift and drag they generate. This enables the turbine to regulate the power extracted from the wind, ensuring efficient operation across a wide range of wind speeds. As the wind speed increases, the pitch angle can be adjusted to reduce the angle of attack of the blades, limiting the power extracted. Conversely, when the wind speed decreases, the pitch angle can be increased to maintain a constant rotor speed and prevent stalling. This dynamic adjustment guarantees optimal turbine operation, regardless of wind conditions.

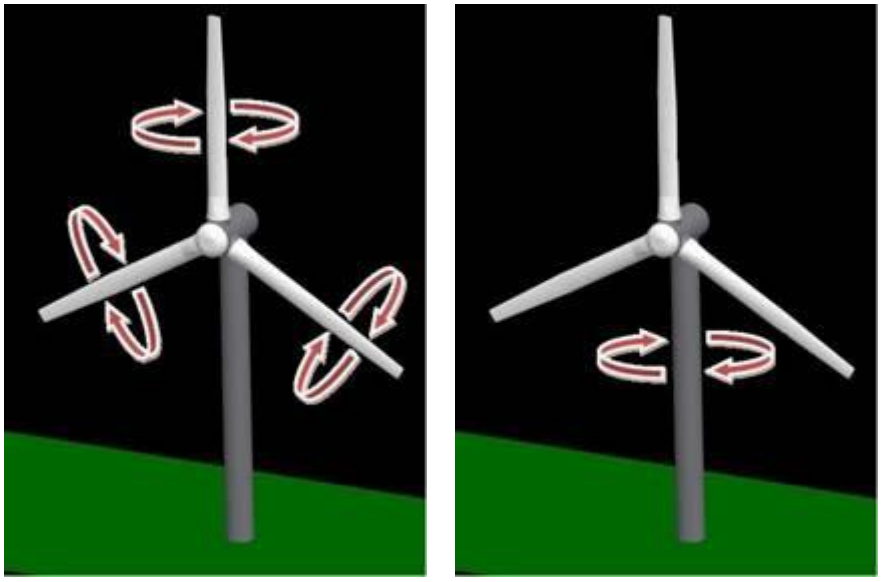

Figure 1.4 Pitch (left) and Yaw (right) control of a wind turbine *[10]*

Finally, Generator Torque Control plays a crucial role in managing wind turbine operations. It involves the precise adjustment of the rotational force applied to the generator shaft, allowing the turbine to regulate power production and maintain the optimal rotor speed. By adeptly increasing or decreasing the generator torque, the turbine can modulate its rotor speed. Importantly, compared to pitch and yaw control methods, torque control has a substantially lower impact on the wind turbine's lifespan [11].

Pitch and yaw control are employed in power regulation for wind turbines. However, to optimize the power captured in the wind, generator torque control is a more suitable option to reduce wear on components [12]. By controlling the rotor speed and maximizing power production, generator torque control effectively enhances the efficiency and longevity of the wind turbine system.

1.4 How does the Generator vary its Torque?

While the primary focus of this thesis is not on building a generator in Simulink, a review of how the generator torque is created provides valuable context and insight for the study's findings.

One effective technique involves the utilization of a doubly-fed induction generator (DFIG) [13], as shown in Figure 1.5. The DFIG is comprised of a partially wound rotor containing two sets of windings: a stator winding and a rotor winding. The stator winding is

linked directly to the grid, while the rotor winding is connected to a converter. The converter is responsible for altering the frequency and voltage of the electrical power that is transmitted into the rotor. By adjusting the electrical power fed into the rotor, the DFIG can regulate its torque output, thus impacting the rotational speed of the turbine. To ensure that the rotor is operating at the optimum speed to produce the highest amount of power, the controller establishes the appropriate voltage.

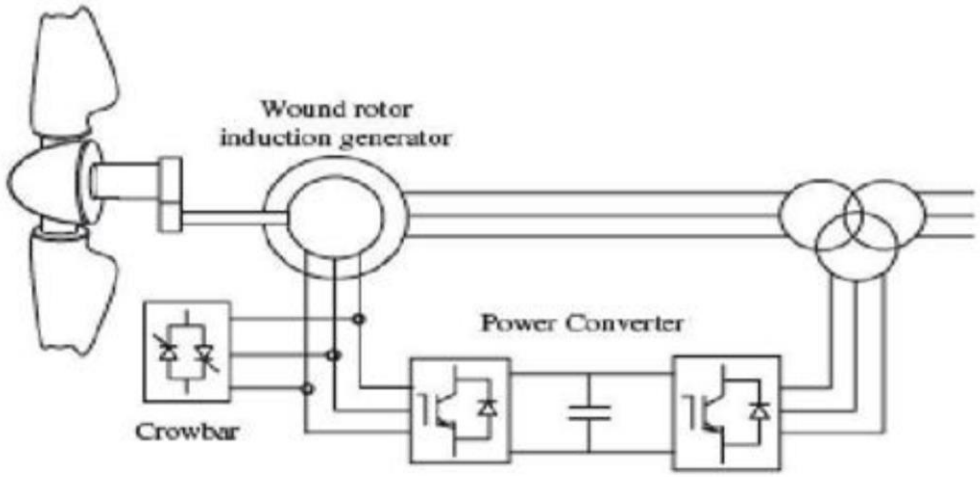

Figure 1.5 Doubly Fed Induction Generator in a wind turbine *[13]*

1.5 Wind Turbine Energy Capture

The wind turbine operates within three specific regions as seen in Figure 1.6 below, each characterized by the wind energy potential that can be captured. These distinct areas showcase the varying efficiency and effectiveness of the turbine system in harnessing energy from the wind, ultimately influencing its overall performance and output.

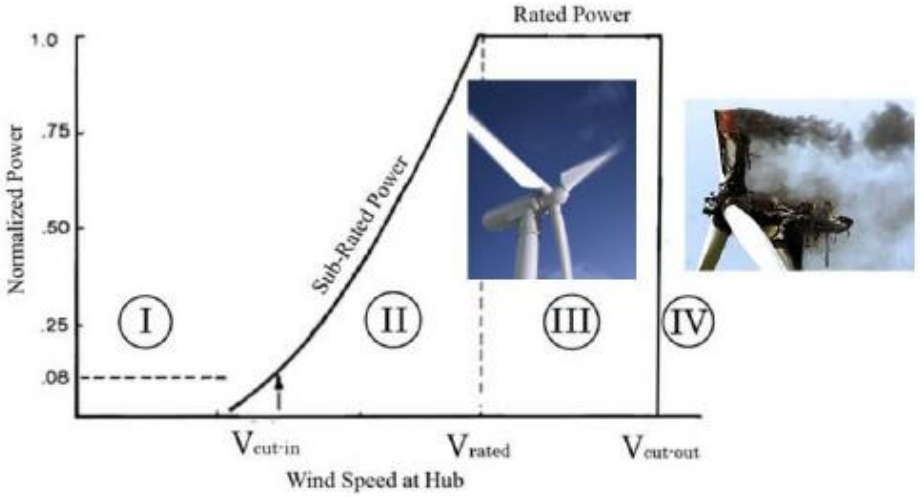

Figure 1.6 Ideal power curve during wind turbine operation *[7]*

In Region I, the low wind speed range is represented, where the turbine does not generate power. During this phase, it is not worth running the wind turbine, as the energy produced does not justify the cost of reducing the life of the turbine. The rotor remains stationary, and no electrical output is produced. This idle state is crucial for preserving the turbine's structural integrity and minimizing unnecessary wear and tear on its components.

Region II is an area where wind energy is abundant and can be utilized to generate electricity. This region, called the power optimization region, aims to capture the maximum amount of kinetic energy from the wind and convert it into electrical energy while minimizing wear and tear on the turbine components. In this region, Maximum Power Point Tracking (MPPT) algorithms are utilized. MPPT controllers dynamically adjust the turbine's rotor speed, ensuring that it operates at the optimal rotor speed corresponding to the maximum power

coefficient. It is important to note that, as seen in Figure 1.7, the maximum power point changes with the wind speed, requiring constant adjustments to maintain optimal performance.

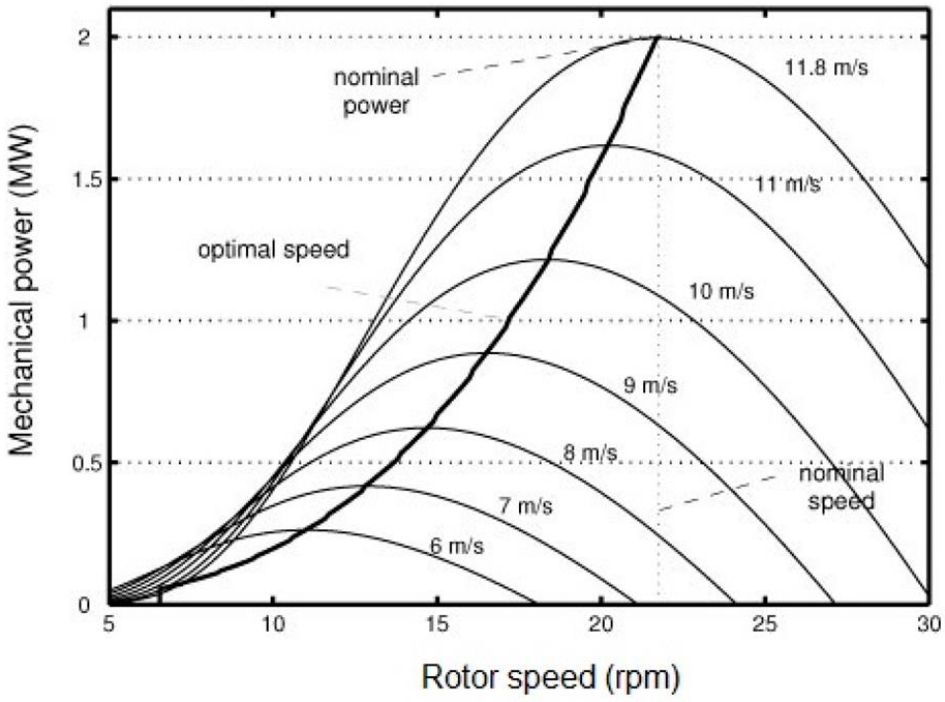

Figure 1.7 Maximum power point tracking region of the wind turbine [7]

Region III, the wind speed is so high that it poses a risk to the turbine's structure. This region, called the power regulation region, is where the goal is to maintain a stable and consistent output of electrical energy by adjusting the rotor speed or blade pitch to match the electrical demand on the grid. In this region, the wind turbine has reached its maximum rated power output. To prevent damage, the turbine is controlled to ensure that it does not overproduce electricity that could damage the turbine. Pitch control adjusts the angle of turbine blades to alter aerodynamic lift and drag forces, shedding excess power ensuring the wind turbine operates within its design limits.

Finally, Region IV refers to wind speeds exceeding the cut-out speed, which is the maximum safe operating speed for wind turbines. The primary objective is to protect the turbine from potential damage caused by extreme wind loads and prevent excessive mechanical stress on components. The turbine control system initiates a shutdown sequence, and once the wind speed returns to a safe range, the turbine resumes operation.

Maximum Power Point Tracking (MPPT) and power regulation are two important techniques used for wind turbine control. MPPT allows the turbine to operate at the maximum power point of the wind turbine's power curve, ensuring that the turbine extracts the maximum energy from the wind. Power regulation, on the other hand, is used to control the output power of the turbine, particularly during periods of high wind speed. By regulating the power output, the turbine can maintain a stable and safe operating condition, preventing damage to the turbine and the power grid. Together, MPPT and power regulation enable wind turbines to operate efficiently and reliably, maximizing power generation and minimizing maintenance costs.

1.6 Scope Assumptions and Limitations

This section includes the considered assumption for modeling and designing control method in next chapters.

- Wind Speed is measurable:

This paper assumes that wind speed is known; however, it is important to note that anemometer readings can be noisy and often misleading due to their location behind the wind turbine. Obtaining true wind speed readings is a challenging task, as various factors contribute to inaccuracies. For instance, the wake effect caused by the turbine blades results in a region of reduced wind speed and increased turbulence downstream. The tower shadow effect also creates a zone of decreased wind speed and heightened turbulence behind the turbine tower. Furthermore, mechanical vibrations from the turbine's moving parts, such as the gearbox and generator, can introduce noise in the wind speed measurements when transmitted to the anemometer.

Wind measurement equipment can have limitations in accuracy and precision, which can lead to errors in wind speed measurements. However, more modern methods are becoming available, such as lidar [14], [15], which can be used to measure wind speed. Remote sensing, multiple anemometers, and advanced data processing techniques also contribute to improved wind speed measurements.

- Generator Torque as an Input:

Although DFIGs are commonly employed for electricity generation, this paper will not delve into modeling a generator; instead, it will assume that the generator is capable of outputting the desired torque. To maintain a degree of realism, the generator input will include a rate limiter to constrain the change in generator torque and a saturation block to simulate the maximum torque that the generator can produce.

- 3rd order Wind Turbine Model:

A wind turbine model was developed on Simulink. This 3rd order wind turbine was used to test the controller. However, compared to an actual wind turbine, it has simplified aerodynamics as well as neglecting some system components. It is also assumed to have rigid components: Some wind turbine models assume that the turbine's main components, such as the blades, tower, and drivetrain, are rigid. This assumption can lead to an underestimation of the system's response to dynamic loads and vibrations.

- FAST:

Compared to the 3rd order wind turbine model, FAST (Fatigue, Aerodynamics, Structures, and Turbulence), a wind turbine simulator, provide a more accurate representation of real-world wind turbines. These simulators play a crucial role in validating controllers before their implementation on actual wind turbines. However, despite their relative accuracy, there are limitations to consider. For example, their aerodynamic models rely on the Blade Element Momentum (BEM) theory [13], which assumes steady flow conditions and often disregards unsteady effects. Consequently, when dealing with intricate flow phenomena like dynamic stall or gusty wind conditions, inaccuracies can arise. Moreover, the simulators employ a multi-body approach to model structural dynamics, treating turbine components as rigid bodies interconnected by flexible joints. While generally effective, this method may not precisely capture the nuanced behavior of the actual structure in certain scenarios. Additionally, the accuracy of simulator predictions heavily relies on the quality and representativeness of the input data, further highlighting the importance of reliable data sources.

1.7 Contributions of Thesis

The goal of this thesis is to develop a controller that will maximize the power generated by the wind turbine in the power optimization region. The contributions of this thesis are listed below:

1. The Maximum Power Point of the turbine is determined through the utilization of a reference tracker. This employs the method of recursive least squares complemented with a forgetting factor. By assuring the optimal tip-speed ratio for wind turbine systems, this strategy enhances power capture from the wind and pinpoints the optimal rotor speed for efficient MPPT.
2. Following that, a First-Order Dynamic Sliding Mode Controller with Integration (FODSMCI) is also implemented. It utilizes generator torque as an input to ensure that the system rotates at the ideal rotor speed.
3. The design of the FODSMCI sliding surface involves the use of hyperplane design to determine the gains. In addition, these gains are optimized to focus on the system's main objective of sliding along the sliding surface.
4. The controller is set to be tested on a wind turbine model that is based on the design principles proposed by Bianchi [7].
5. This is followed by an evaluation using the wind turbine simulator known as FAST, which is certified by the National Renewable Energy Laboratory (NREL) [16].
6. The controllers are then compared in terms of actuation energy, tracking performance, and robustness.

1.8 Organization of Thesis

The thesis is organized as follow:

- Chapter 1

The opening chapter of the thesis offers a comprehensive understanding of Wind Energy Conversion Systems. An encompassing overview of the wind turbine system is presented, focusing on its operating regions and how these mechanisms are controlled. This chapter also outlines the overall scope and assumptions that underpin the thesis and describes the distinctive contributions that the work brings to the field.

- Chapter 2

In the second chapter, the thesis takes a deep dive into a literature review. This part focuses on current MPPT methods, and a range of control methods utilized in wind turbine management. A key focus here is Sliding Mode Control - exploring its foundational principles and discussing the modifications that make it suitable for application in wind turbines.

- Chapter 3

The third chapter is where the development of the reference tracking and controller methods takes place. The Recursive Least Square Method is introduced as a tool to pinpoint the Maximum Power Point of the turbine. A novel technique, based on Sliding Mode Control, is proposed as the controller method. Simultaneously, a simple wind turbine model is constructed for testing purposes. This chapter also explains how model validation occurs using FAST, a wind turbine simulator, and how TurbSim is employed for wind generation.

- Chapter 4

The fourth chapter presents the results derived from the methodologies outlined in the preceding section. Here, the methods are put to the test on two models - a Simple Wind Turbine Model and the FAST models.

- Chapter 5

The fifth and final chapter serves to summarize the entirety of the work. This conclusion encapsulates the main points and outcomes of the research, painting a clear picture of the findings. Furthermore, the final section provides recommendations for future research, indicating potential directions for subsequent investigations in the field of wind energy conversion systems.

Chapter 2 Literature Review

In this chapter, an exploration of the diverse range of reference tracking techniques is conducted to pinpoint the Maximum Power Point Tracking (MPPT) point and controller methods, shedding light on the underlying motivations that inspired the development of this paper.

2.1 Reference Tracking Methods

The power curve is a crucial concept that illustrates the relationship between wind speed and the power output of a wind turbine. The curve exhibits a peak where the turbine generates maximum power for a given wind speed. MPPT is a control algorithm used in wind turbines to optimize their power output by finding the peak of this power curve. By achieving this, the turbines can operate at the most efficient point, resulting in increased energy production. To achieve this, reference tracking can be used, which is focused on determining the optimal Tip Speed Ratio (TSR) to maximize power generation.

The simplest method for determining the optimal TSR involves either experimental or theoretical approaches [17]. Using this optimal TSR, the rotor can be designed to operate under ideal conditions. However, a limitation exists as the accumulation of dirt, ice, or snow on the rotor blades can alter their lift characteristics, which in turn can affect the optimal TSR and overall performance of the wind turbine. As the aerodynamic properties of the blades change, the optimal TSR may shift, leading to reduced efficiency and power output.

The Perturb and Observe (P&O) [18], [19] method, as shown in Figure 1.2 is technique that perturbs the operating point of the wind turbine and observes the resulting change in power output. The controller adjusts the operating point in the direction of the change that leads to the maximum power output. However, this method has its own drawbacks. The P&O method may be sensitive to noise in measurements, may not always converge to the true maximum TSR, and can take a long time to converge to the Maximum Power Point.

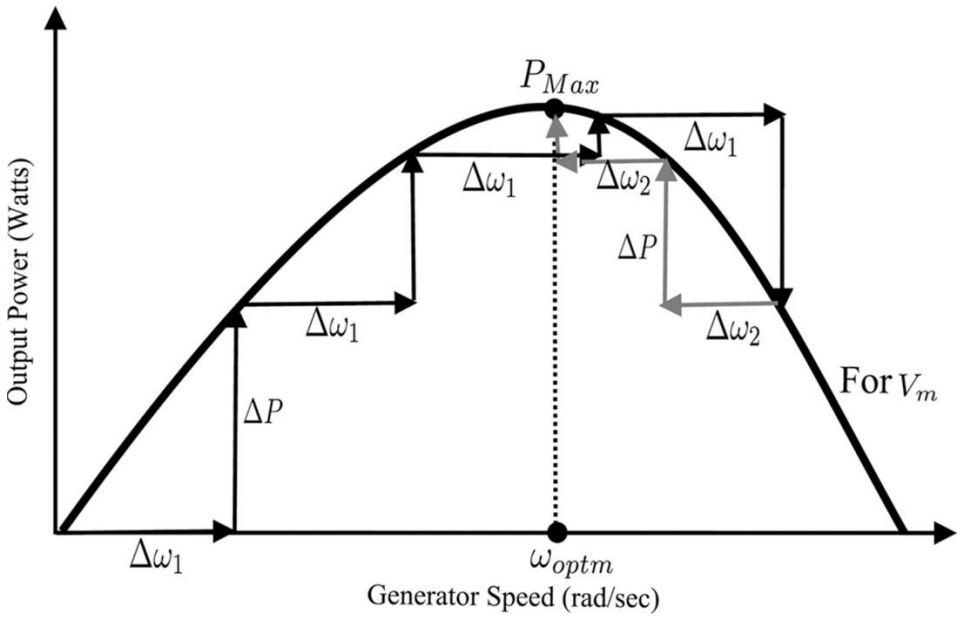

Figure 2.1 Perturb and Observe used to find the operating curve of the wind turbine [20]

The Incremental Conductance (INC) [21] Method utilizes the derivative of the power-voltage curve to determine the direction of the maximum power point. This method proves to be more accurate than the P&O method and is less likely to cause oscillations, but it is more complex to implement. Additionally, the INC method can be sensitive to changes in wind speed and is computationally more demanding than the P&O method.

The Hill-Climbing (HC) Method [22], [23], incrementally adjusts the operating point of the wind turbine in the direction of the maximum power output until the maximum power point is reached. However, this method may not be suitable for rapidly changing wind conditions and may result in oscillations around the maximum power point.

Model Predictive Control (MPC) [24] is an advanced control strategy that uses a model of the system to predict future system behavior and determine the optimal control actions. In the context of MPPT for wind turbines, MPC can optimize the operating point by solving an optimization problem over a finite prediction horizon. MPC offers adaptability and robustness compared to other MPPT methods. However, its performance depends heavily on the accuracy of the system model, and its computational complexity can be demanding.

2.2 Controller Methods

The main objective of a wind turbine controller is to ensure that the turbine rotor speed is at the ideal point, which will yield the maximum amount of power, particularly in Region II of the turbine's power curve. In the context of this paper, the wind turbine rotation speed should be maintained at the ideal TSR. Various control techniques have been explored to achieve this objective, including Proportional-Integral-Derivative control, Linear Quadratic Regulator control, gain scheduling, and fuzzy logic control. Each of these methods has its advantages and drawbacks, which influence their suitability for specific wind turbine applications.

Proportional-Integral-Derivative (PID) [25]. control offers simplicity, ease of implementation, cost-effectiveness, and the ability to minimize overshoot and oscillations. However, tuning the control parameters to achieve the desired performance can be both time-consuming and challenging, further highlighting some of the issues associated with PID control in wind turbine applications.

Linear Quadratic Regulator (LQR) [26] [27]. control is a technique frequently employed to optimize the performance of wind turbines by adjusting the blade pitch angle. LQR controllers are designed to modify the blade pitch angle in real-time based on measurements of wind speed and other operating parameters, offering a more sophisticated control compared to PID as it is capable of handling Multiple-Input-Multiple-Output (MIMO) systems. However, LQR control faces several challenges when applied to wind turbine control. One significant challenge is the highly nonlinear nature of the wind turbine system, as the aerodynamic characteristics constantly change, making it difficult to accurately model the system. Additionally, disturbances such as gusts of wind or turbulence can cause deviations from the desired performance, potentially leading to instability or decreased energy production.

Gain scheduling [7] is a control strategy used to improve the performance of wind turbines by adjusting the controller gains based on the current operating conditions. This method can improve the efficiency and reliability of wind turbines, and it is particularly useful for large-scale wind farms where the operating conditions can vary significantly across the farm. However, gain scheduling can increase the complexity of the control system, which can make it more difficult to design, implement, and maintain. The need for additional sensors and

computational resources can also increase the cost of the control system. Furthermore, the gain scheduling algorithm requires tuning, which can be a time-consuming process, and may also require frequent recalibration to ensure optimal performance.

Fuzzy logic control (FLC) [28] [29] uses a set of rules that define the relationship between the input variables, such as wind speed and rotor speed, and the output variables, such as pitch angle and generator torque. FLC can improve the efficiency and reliability of wind turbines, particularly in conditions where other control strategies may be less effective, such as low wind speed or high turbulence. However, the process of fuzzification, rule evaluation, and defuzzification can require a significant amount of computational power, which may be a limitation in some applications. Additionally, the relationship between the input variables and the output in FLC can be difficult to understand. This can be a problem in wind turbine control applications where a clear understanding of the control system is necessary for decision-making.

Common practice for wind turbine control methods as mentioned above involves using a linearization approach. This simplifies the complex nonlinear dynamics of wind turbines, allowing for easier design and analysis of control systems. Well-established linear control methods can be easily implemented, and these algorithms are computationally efficient, suitable for real-time control applications and large-scale wind farm simulations. However, there are drawbacks. Linear models, being approximations of the actual nonlinear system, may have limited accuracy when operating conditions deviate significantly from the linearization point, leading to reduced performance and system reliability. In the face of stochastic operating conditions and inherent uncertainties, nonlinear and robust control methods are needed to better accommodate the complexities of wind turbine systems and improve overall performance and reliability.

2.3 Sliding Mode Control

In this thesis, the application of Sliding Mode Control (SMC) to regulate the generator speed of a wind turbine by adjusting its torque will be explored. SMC is a robust nonlinear control technique that effectively handles disturbances and uncertainties in wind and system dynamics. It has already been implemented in several commercial wind turbines due to its numerous benefits, such as robustness, finite-time convergence, and reduced-order compensated dynamics [30].

The core concept of sliding mode control involves designing a control law that drives the system states to slide along a prescribed surface, defined as a linear combination for the state variables. This sliding surface (manifold) is determined by the difference between the desired output and the actual output, ensuring that system states converge to the surface from any initial condition. Furthermore, the motion along the surface remains insensitive to disturbances and uncertainties, allowing for more reliable and stable control.

In SMC, there are two distinct phases [30] as shown in Figure 2.2. The initial phase, known as the Reaching phase, involves propelling the system from its starting condition towards the manifold. This is accomplished by ensuring that $\frac{dL}{dt} < 0$, with $L = \frac{1}{2}s^2$ (Lyapunov condition) being a common choice. Following this, the system enters the Sliding phase, during which it moves along the manifold ($s = 0$) toward the origin. This sliding motion is facilitated by the stable dynamics resulting from the carefully chosen parameters for $s = Cx$ in the linear combination of the surface.

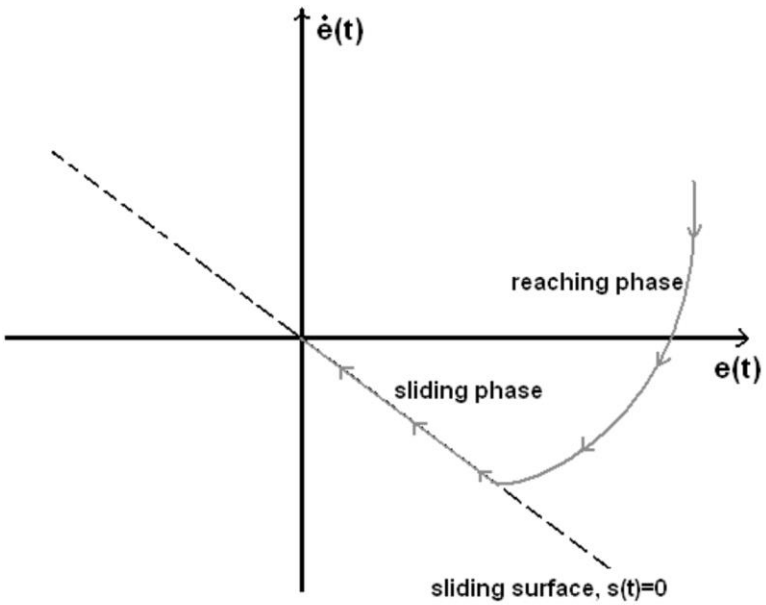

Figure 2.2 Phase portrait showing Reaching and Sliding Phase of SMC *[31]*

However, SMC does come with its challenges, the most notable being chattering. Chattering arises from the rapid switching of the control input near the sliding surface due to the use of a discontinuous function as seen in Figure 2.3. This phenomenon can lead to high-frequency oscillations in the system output, potentially degrading performance and causing excessive wear and tear on mechanical components. In the context of wind turbines, chattering can have devastating consequences [32].

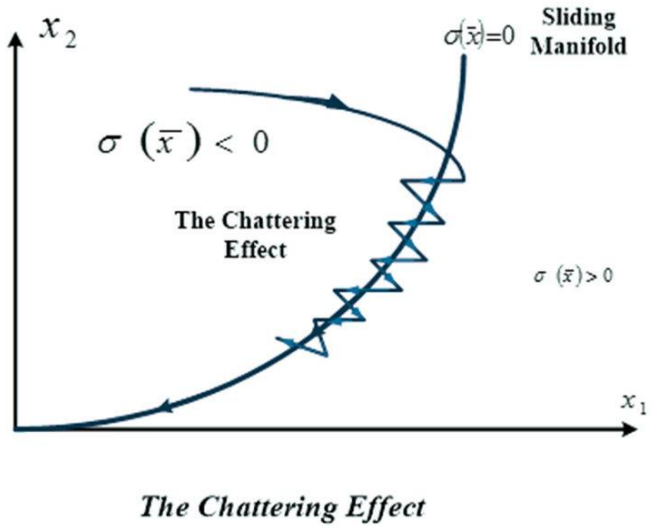

Figure 2.3 Example of Chattering along the Sliding manifold when using SMC *[33]*

To overcome the issue of chattering in sliding mode control, several methods have been proposed in the literature. These methods aim to maintain the robustness and efficiency of sliding mode control while minimizing the adverse effects of chattering on system performance and component wear. One method is to use Integral sliding mode [34] on wind turbines. In this approach, an integral sliding mode power controller is adopted, which not only ensures the robustness of the system but also reduces the steady-state error of rotor speed and the load on the transmission system. By integrating the sliding surface, the control law can be designed to reduce chattering and improve overall system performance.

Another method to mitigate chattering is adding boundary layer [35] around the sliding surface. One of the key components of boundary layer SMC is the use of a saturation function or a hyperbolic tangent function to design the sliding mode controller. The saturation function is used to limit the control signal to a predefined maximum value, while the hyperbolic tangent function ensures smooth control signal transitions during sliding mode operation. The combination of these functions provides a robust and efficient control strategy for systems with significant uncertainties, while reducing chattering.

Having a High-Order Sliding Mode Control [36] of wind turbines is another method proposed to address chattering [16]. This control strategy involves the use of a high order sliding mode controller to ensure stability in both operation regions and to impose the ideal feedback control solution despite model uncertainties. The proposed control strategy combines a second order sliding mode observer to increase the order of the system, followed by the implementation of a second-order sliding mode controller. Validation results show that the proposed control strategy is effective in terms of power regulation, and the torque generator remains smooth. Moreover, the high order sliding mode approach produces no chattering in the generated torque. However, this method does increase the complexity of the system, which may present challenges in terms of implementation and computational requirements.

Finally, an alternative way to minimize chatter is using First Order Dynamic Sliding Mode Control [37]. This method offers several advantages, such as the construction of a new sliding surface using a linear combination of system states and controls, rather than relying solely on states allowing for greater flexibility in designing sliding surfaces and specifying closed-loop dynamics. Furthermore, the solution for a controller that achieves a sliding condition in closed-

loop dynamics results in a dynamic compensator with first-order dynamics. This approach effectively filters the error signal before it is passed on to the actuator, causing the sliding mode controller to exhibit no chattering in the response. The foundation of this thesis is built upon the principles presented in this paper.

Chapter 3 Development of Methods

This thesis builds upon the paper [38] presented at the 10th International Conference of Control Systems, Dynamic Systems, and Robotics (CDSR'23), which took place from June 1-3, 2023, in Ottawa, Canada. Further depth and additional details will be provided in the following discussion to enhance understanding of the ideas and research outlined in that paper.

Figure 3.1 below illustrates the implementation on how the system will be implemented:

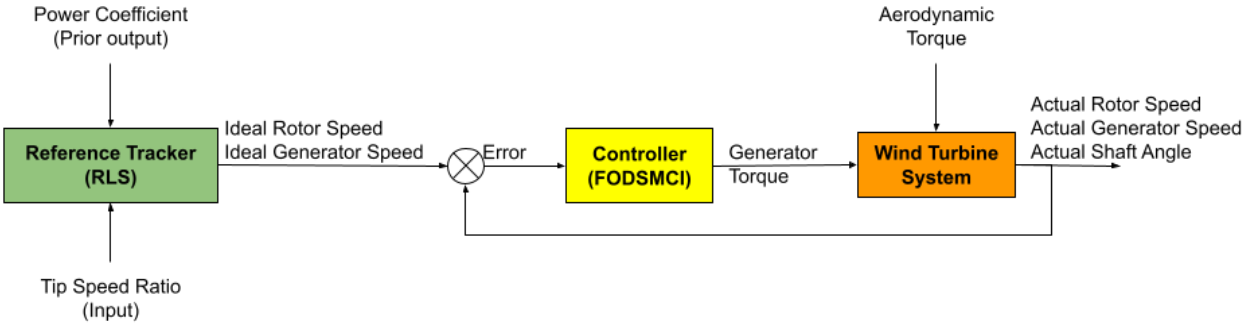

Figure 3.1 Schematic of this system that will be implemented

The figures above present the reference tracking and controller setup for a wind turbine system. The problem focuses on regulating the rotor speed of a wind turbine at the optimal Tip speed ratio (TSR) using generator torque. The TSR represents the ratio of the rotor speed to the incoming wind speed, indicating the point at which the wind turbine can extract the maximum energy from the wind. Maintaining the rotor speed at the optimal TSR ensures peak efficiency, maximizing the electrical power generated from available wind energy. The optimal TSR is determined by using the Recursive Least Squares (RLS) with a forgetting factor. Then achieve accurate and robust control in uncertain wind conditions, the First Order Dynamic Sliding Mode controller with integration is implemented. This control system keeps the rotor speed sliding along the optimal TSR curve, adjusting the generator torque to match varying wind conditions. This approach not only maximizes energy production but also reduces mechanical stress on the wind turbine, enhancing its overall efficiency.

3.1 Reference Tracking using the Recursive Least Squares with a Forgetting Factor

Recursive least squares (RLS) is a linear model parameter estimation algorithm that updates estimates using recent data. It has fast convergence rate and is well suited for online learning. RLS is also robust to noise. It is useful in determining the optimal Tip Speed Ratio (TSR) for a wind turbine, enabling the identification of the Maximum Power Point (MPP) of the turbine.

This thesis assumes that the results obtained from the wind turbine system are in continuous time. However, RLS requires sampled data. To minimize computational complexity while preserving the accuracy of TSR estimation, a sampling period (T_s) will be chosen.

Estimating the power curve holds immense importance in wind energy engineering applications. Relying solely on the published approximate power curve oversimplifies the intricate nature of its behavior and leads to limitations in its accuracy. The power curve demonstrates significant temporal variability, influenced by various factors such as wind speed, wind acceleration, rotor acceleration, and the possibility of higher order derivatives. When examining instantaneous measurements of the power coefficient relative to tip speed ratio, a cloud-like graph emerges, highlighting the dynamic relationship between these parameters, as illustrated in Figure 3.2 below:

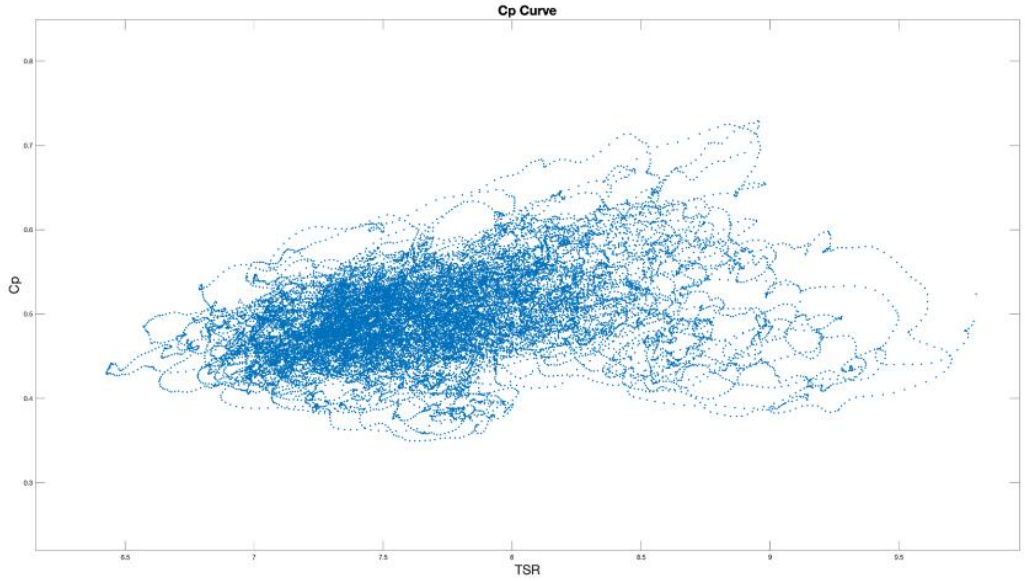

Figure 3.2 The power coefficient from a simulation of NREL FAST's 5MW reference turbine [39].

An estimation approach is needed to capture the level of detail and variability in the power curve. Comprehensive estimation allows insights into the transient behavior of wind turbine systems, enabling optimized energy production strategies. The method of implementing RLS with a forgetting factor will be based on the work of Vahidi et al [40].

The input used in this method will be the TSR (λ), and the output will be the Aerodynamic Power Coefficient (C_P) for the polynomial equation:

$$C_p(i) = \alpha_m \lambda_i^m + \alpha_{m-1}\lambda_i^{m-1} + \cdots + \alpha_2 \lambda_i^2 + \alpha_1 \lambda_i + \alpha_o \tag{3.1}$$

Where α_m is the coefficients. Then, initialize the covariance matrix ($\boldsymbol{P}$), input vector ($\boldsymbol{\sigma}$), and estimated parameters vector ($\widehat{\boldsymbol{\theta}}$) [41]:

$$\boldsymbol{P} = \delta \begin{bmatrix} 1 & \cdots & 0 \\ \vdots & \ddots & \vdots \\ 0 & \cdots & 1 \end{bmatrix}, \boldsymbol{\sigma} = \begin{bmatrix} \lambda_i^m \\ \lambda_i^{m-1} \\ \vdots \\ \lambda_i^1 \\ 1 \end{bmatrix}, \widehat{\boldsymbol{\theta}} = \begin{bmatrix} \alpha_m \\ \alpha_{m-1} \\ \vdots \\ \alpha_1 \\ \alpha_o \end{bmatrix} = \begin{bmatrix} 0 \\ 0 \\ \vdots \\ 0 \\ 0 \end{bmatrix} \tag{3.2}$$

Where $\delta = 100$. Then update the parameter gain value K:

$$\boldsymbol{K} = \frac{\boldsymbol{P}(i-1)\boldsymbol{\sigma}}{\mu + \boldsymbol{\sigma}^T \boldsymbol{P}(i-1)\boldsymbol{\sigma}} \tag{3.3}$$

Calculate the covariance matrix:

$$\boldsymbol{P}(i) = \frac{\boldsymbol{P}(i-1)}{\mu}(\boldsymbol{I}(m+1) - \boldsymbol{K}\boldsymbol{\sigma}^{\boldsymbol{T}}) \tag{3.4}$$

The forgetting factor (μ) in Eqs. (3.3) and (3.4) is a parameter that determines the weight given to new data. It typically ranges from 0.9 to 1, with lower values indicating that only more recent data should be trusted, while a value of 1 indicates that all data points should be treated equally. The weight given to past data is determined by the exponential decay function, where *j* is the number of steps into the past and μ^j is the weight assigned to that data point.

$$\widehat{\boldsymbol{\theta}}(i) = \widehat{\boldsymbol{\theta}}(i-1) + \boldsymbol{K}(y(i) - \boldsymbol{\sigma}^{\boldsymbol{T}}\widehat{\boldsymbol{\theta}}(i-1)) \tag{3.5}$$

To find the λ that yields the maximum power, the derivative of the power coefficient polynomial (Eqs. (3.1)) with respect to λ is taken and set equal to zero:

$$\frac{dC_p(i)}{d\lambda} = \alpha_m m * \lambda^{m-1} + \alpha_{m-1} * (m-1) * \lambda^{m-2} + \cdots + \alpha_2 * 2 * \lambda + \alpha_1 = 0 \tag{3.6}$$

In this study, a third-order ($m = 3$) polynomial was utilized as the chosen model. This was done to simplify the process of determining the λ that yields the maximum C_P value However, it is important to note that a more comprehensive analysis may be necessary to explore different model orders and fully understand their performance and suitability. Therefore, the third-order polynomial will be:

$$3\alpha_3\lambda^2 + 2\alpha_2\lambda + \alpha_1 = 0 \tag{3.7}$$

λ can be found the using quadratic equation:

$$\lambda = \frac{-\alpha_2 \pm \sqrt{\alpha_2^2 - 3\alpha_1\alpha_3}}{3\alpha_3} \tag{3.8}$$

Since Eqs. (3.8) will give two solutions, pick the positive one, as the TSR is always positive. Repeat this entire process for the next sample data with the new $\widehat{\boldsymbol{\theta}}$ and next $\boldsymbol{\sigma}$.

3.2 First Order dynamic SMC with integration as the Controller

This thesis will a variation of be using a Sliding mode control (SMC). This is used over other controllers like PID due to its superior robustness. SMC guarantees inherent stability and effective disturbance rejection, even when external disturbances and uncertainties are present. One of its key strengths lies in its exceptional performance in highly nonlinear systems, offering precise and reliable control—a significant advantage over PID control, which may face limitations in linear systems. SMC is particularly adept at handling model uncertainties and variations within a system. By implementing sliding mode techniques, SMC successfully eliminates steady-state errors, enabling accurate tracking of reference signals and enhancing overall control accuracy.

The SMC method used in this paper will be thee first-order dynamic sliding mode control with integration (FODSMCI). This modified model is based on the work of Pieper [37]. The first-order dynamics of the controller filter the error signal, eliminating chattering at the actuator as a result. This is achieved by incorporating an integral term directly into the sliding function, which eliminates steady-state errors and compensates for persistent disturbances. Additionally, linear quadratic optimal design conditions can be used to select the sliding surface vector parameter. The primary objective of this thesis is to control the wind turbine rotor speed solely through the generator torque, aiming to maintain it at the optimal Tip Speed Ratio (TSR).

To start, the controllable portion of the system is needed:

$$\dot{\boldsymbol{x}} = \boldsymbol{A}\boldsymbol{x} + \boldsymbol{B_c}u \tag{3.9}$$

Where $\boldsymbol{A}$ is the state matrix, $\boldsymbol{B_c}$ is the controllable portion of the input matrix, $\boldsymbol{x}$ represents the state vector, and u is the input vector. In the case of the wind turbine, u corresponds to the generator input torque.

As for the sliding surface, it will be similar to the one described in [33], with the inclusion of an additional integral term as shown:

$$s = \boldsymbol{C_1}\boldsymbol{x} + C_2\int \boldsymbol{C_1}\boldsymbol{x} + Du \tag{3.10}$$

Where $\boldsymbol{C_1}$ is the sliding gains of the state and C_2 is the sliding gain for the integral term. Due to the addition of an integral term, the method outlined in [37] requires modification and solved using iteration.

Then, to find the control model, take the derivative of Eqs. (3.10):

$$\dot{s} = \boldsymbol{C_1}\dot{\boldsymbol{x}} + C_2\boldsymbol{C_1}\boldsymbol{x} + D\dot{u} \tag{3.11}$$

And substitute in Eqs. (3.9). Finally, isolate for $D\dot{u}$:

$$D\dot{u} = -\boldsymbol{C_1}\boldsymbol{A}\boldsymbol{x} - \boldsymbol{C_1}\boldsymbol{B_c}u - C_2\boldsymbol{C_1}\boldsymbol{x} + \dot{s} \tag{3.12}$$

Where $\dot{s}$ is the sliding condition which can be derived using the Lyapunov stability theory. First, the candidate Lyapunov function takes the form:

$$V = \frac{1}{2}s^2 \tag{3.13}$$

For Eqs. (3.11) to have asymptotic stability about the equilibrium $s = 0$, the following conditions must be satisfied[30]:

$$\begin{aligned} &a) \quad \lim_{|\sigma|\to\infty} V \to \infty \\ &b) \quad \dot{V} < 0 \text{ for } \sigma \neq 0 \end{aligned} \tag{3.14}$$

Condition (a) is satisfied by inspecting Eqs. (3.13) as it will always be positive and will go toward infinity as s increases. Then, in order to achieve finite-time stability, condition (b) can be modified to be[30]:

$$\dot{V} \leq -\eta\sqrt{2V} \tag{3.15}$$

Where η is the sliding gain is $\eta > 0$. Then substitute Eqs. (3.13) into (3.15):

$$\dot{V} \leq -\eta|s| \tag{3.16}$$

Then take the derivative of Eqs. (3.13):

$$\dot{V} = s\dot{s} \tag{3.17}$$

Combine Eqs. (3.16) and (3.17), and reorganize for $s\dot{s}$ which give the reachability condition:

$$s\dot{s} < -\eta|(s)| \tag{3.18}$$

The sliding mode condition ($\dot{s}$) defined by satisfying the reachability condition [42] as shown in Eqs. (3.18). Therefore, the sliding mode condition will be:

$$\dot{s} = -\eta * sign(s) \tag{3.19}$$

It can be assumed that $D \neq 0$ and further, without loss of generality that $D = 1$. Then by combining Eqs. (3.12) and (3.19), the controller can be reformed as a first order differential equation as:

$$\dot{u} = -\boldsymbol{C_1 A x} - \boldsymbol{C_1 B_c} u - C_2 \boldsymbol{C_1 x} - \eta * sign(s) \tag{3.20}$$

3.2.1 Hyperplane Design for First Order Dynamic Sliding Mode with Integration

To find C_1 and C_2, it is assumed that the system is on the sliding surface where $s = 0$. An integral of the states is also introduced as $\dot{x}_i = C_1 x$, which when combined, yields:

$$\begin{bmatrix} \dot{\boldsymbol{x}} \\ \dot{\boldsymbol{x}}_{\boldsymbol{i}} \\ \dot{u} \end{bmatrix} = \begin{bmatrix} \boldsymbol{A} & 0 & \boldsymbol{B} \\ \boldsymbol{C_1} & 0 & 0 \\ -\boldsymbol{C_1 A} - C_2 \boldsymbol{C_1} & 0 & -\boldsymbol{C_1 B_c} \end{bmatrix} \begin{bmatrix} \boldsymbol{x} \\ \boldsymbol{x}_{\boldsymbol{i}} \\ u \end{bmatrix} \tag{3.21}$$

To use the Hyperplane design method in [43], Eqs. (3.21) above needs to be transformed:

$$\begin{bmatrix} \dot{\boldsymbol{x}}_{\boldsymbol{s}} \\ \dot{u} \end{bmatrix} = \begin{bmatrix} \boldsymbol{A_a} & \boldsymbol{B_a} \\ -\boldsymbol{C_a A_a} & -\boldsymbol{C_a B_a} \end{bmatrix} \begin{bmatrix} \boldsymbol{x_s} \\ u \end{bmatrix} \tag{3.22}$$

where:

$$\boldsymbol{A_a} = \begin{bmatrix} \boldsymbol{A} & 0 \\ \boldsymbol{C_1} & 0 \end{bmatrix}, \boldsymbol{B_a} = \begin{bmatrix} \boldsymbol{B_c} \\ 0 \end{bmatrix}, \boldsymbol{C_a} = [\boldsymbol{C_1} \quad C_2], \boldsymbol{x_s} = \begin{bmatrix} \boldsymbol{x} \\ \boldsymbol{x_i} \end{bmatrix} \tag{3.23}$$

The state space of Eqs. (3.22) is written as:

$$\dot{\boldsymbol{x}}_{\boldsymbol{s}} = \boldsymbol{A_a x} + \boldsymbol{B_a} u \tag{3.24}$$

Then quadratic performance index [37], [43] is chosen as:

$$J = \int_0^\infty [\boldsymbol{x_s^T} \quad \boldsymbol{u^T}] \begin{bmatrix} \boldsymbol{H_{11}} & \boldsymbol{H_{12}} \\ \boldsymbol{H_{21}} & R \end{bmatrix} \begin{bmatrix} \boldsymbol{x_s} \\ u \end{bmatrix} dt \tag{3.25}$$

$\boldsymbol{H_{11}}$ and R are positive semi-definite matrices that are used to weigh the importance of the states and control inputs for the performance index. $\boldsymbol{H_{11}}$ determines how much the control strategy should attempt to minimize the deviation of the states from their desired values. R determines how much the control strategy should try to minimize the control effort. The cost function, Eqs. (3.25), can be minimized using the Algebraic Riccati Equation (ARE) [44]:

$$\boldsymbol{S A_a + A_a^T S - S B_a} R^{-1} \boldsymbol{B_a^T S + H_{11}} = 0 \tag{3.26}$$

Where $\boldsymbol{A_a}$ and $\boldsymbol{H_{11}}$ are the state transition matrix and the state weighting matrix, respectively. However, in order to minimize Eqs. (3.25), the cross-product terms ($\boldsymbol{H_{12}}$ and $\boldsymbol{H_{21}}$) need to be considered since they are generally non-zero. To account for the cross-product terms in the cost function, first define the pseudo control input:

$$v = u + R^{-1} \boldsymbol{H_{12}^T x_s} \tag{3.27}$$

Then, input the equation into state space model, Eqs. (3.24):

$$\boldsymbol{\dot{x} = A_a x_s + B_a} (v - R^{-1} \boldsymbol{H_{12}^T x_s}) \tag{3.28}$$

Rearrange Eqs. (3.28):

$$\dot{x} = (\boldsymbol{A_a - B_a} R^{-1} \boldsymbol{H_{12}^T}) \boldsymbol{x_s + B_a} v \tag{3.29}$$

Therefore, the new state transition matrix will be:

$$\boldsymbol{F^*} = \boldsymbol{A_a - B_a} R^{-1} \boldsymbol{H_{21}} \tag{3.30}$$

Next, to determine the new state weighting matrix, first expand Eqs. (3.25):

$$J = \int_0^\infty (\boldsymbol{x_s^T H_{11} x_s} + \boldsymbol{u}^T R u + 2 \boldsymbol{x}^T \boldsymbol{H_{12}} u) dt \tag{3.31}$$

Then, input Eqs. (3.27) into Eqs. (3.31):

$$\begin{aligned} J = \int_0^\infty (\boldsymbol{x_s^T H_{11} x_s} + (v - R^{-1} \boldsymbol{H_{12}^T x_s})^T R (v - R^{-1} \boldsymbol{H_{12}^T x_s}) \\ + 2 \boldsymbol{x}^T \boldsymbol{H_{12}} (v - R^{-1} \boldsymbol{H_{21} x_s})) dt \end{aligned} \tag{3.32}$$

Then expand the equation:

$$J = \int_0^\infty (\boldsymbol{x_s^T}\, \boldsymbol{H_{11}} \boldsymbol{x_s} + v^T R v - v^T \boldsymbol{H_{12}} \boldsymbol{x_s} - \boldsymbol{x_s^T} \boldsymbol{H_{21}} v + \boldsymbol{x_s^T} \boldsymbol{H_{21}} R^{-1} \boldsymbol{H_{12}} \boldsymbol{x_s} + 2\boldsymbol{x_s^T} \boldsymbol{H_{12}} v - 2\boldsymbol{x_s^T} \boldsymbol{H_{12}} R^{-1} \boldsymbol{H_{21}} \boldsymbol{x_s}) dt \tag{3.33}$$

Collect the like terms:

$$J = \int_0^\infty \boldsymbol{x_s^T}\, (\boldsymbol{H_{11}} - \boldsymbol{H_{21}} R^{-1} \boldsymbol{H_{21}}) \boldsymbol{x_s} + v^T R v \tag{3.34}$$

Then, the updated state weighting matrix is given as:

$$\mathbf{R}^* = \boldsymbol{H_{11}} - \boldsymbol{H_{12}} R^{-1} \boldsymbol{H_{21}} \tag{3.35}$$

Now, with the new state transition matrix (Eqs. (3.30)) and state weighting matrix (Eqs. (3.35)), the ARE can be used to solve for $\boldsymbol{S}$ [37]:

$$\boldsymbol{S F^*} + \boldsymbol{F^{*T} S} - \boldsymbol{S B_a} R^{-1} \boldsymbol{B_a}^{\boldsymbol{T}} \boldsymbol{S} + \boldsymbol{R^*} = 0 \tag{3.36}$$

Once the solution has been obtained, the coordinates are transformed back to the original ones to obtain the pseudo-control shown below, which serves as the choice of sliding mode defining vector:

$$\boldsymbol{C_a} = R^{-1}\left(\boldsymbol{H_{21}} + \boldsymbol{B_a}^{\boldsymbol{T}} \boldsymbol{S}\right) \tag{3.37}$$

However, since $\boldsymbol{A_a}$ is function of $\boldsymbol{C_1}$, which is part of $\boldsymbol{C_a}$, the system needs to be solved iteratively until the sliding surface ($\boldsymbol{C_a}$) gain converges to the stopping criteria, as shown:

$$\left| max\left(\boldsymbol{C_a}(i)\right) - max\left(\boldsymbol{C_a}(i-1)\right) \right| > 0.01 \tag{3.38}$$

This stopping criterion is represented in the first row of Figure 3.3, where the difference between the maximum value of $\boldsymbol{C_a}$ in the current iteration and the previous iteration is plotted against the iteration number. If this difference falls below 0.01, the iterative process is stopped, indicating that the solution has approximately converged. However, if it does not converge in 100 iterations or diverges, then the cost function was not able to be minimized properly. Therefore, proper weights ($H_{11}$and R) need to be selected to meet the stopping criteria to minimize the cost function (Eqs. (3.25))

3.2.2 Minimizing the Cost Function along the Sliding Surface

To improve the results, the cost function can be to minimize along the sliding surface. This is done by redefining the weights :

$$\boldsymbol{H_{11} = C_a^T C_a} \tag{3.39}$$

Repeat the process from Eqs. (3.23) to (3.37) until $\boldsymbol{C_a}$ reaches the stopping criteria(Eqs. (3.38)) as shown in Figure 3.3 below:

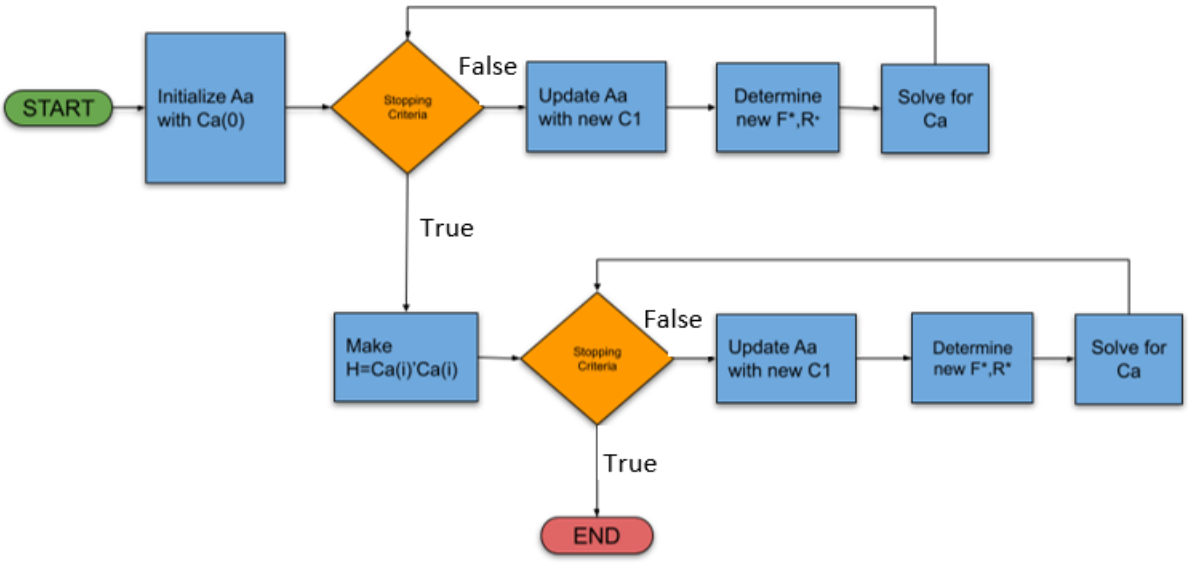

Figure 3.3 Flow chart on solving for the Sliding surface gains ($\boldsymbol{C_a}$)

The aim is to make the rotor speed track the optimal rotor speed to maximize power generation, while also reducing the usage of generator torque to extend the life of the turbine. However, this introduces a trade-off as reducing the usage of generator torque will lower the rotor speed tracking, thus reducing power.

3.3 Mass Spring Damper Example

This section will demonstrate the FODSMCI to control the position of the Mass Spring damper (MSD). Consider the MSD diagram:

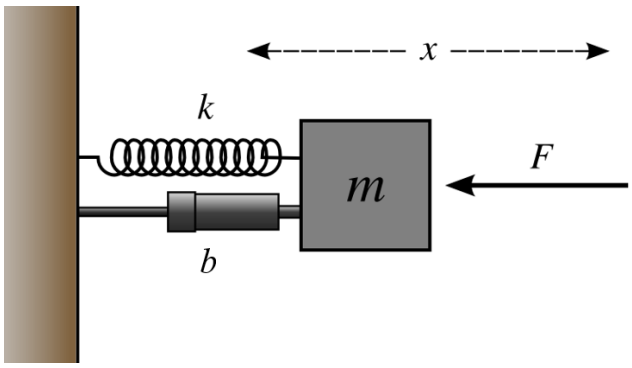

Figure 3.4 Mass spring damper diagram

Where k is the spring constant, B is damping constant, and m is the mass give the differential equation as:

$$m\ddot{x} + b\dot{x} + kx = F \tag{3.40}$$

F is the external force, where:

$$F = u + w \tag{3.41}$$

Where u and w is the control and disturbance input force respectively. Therefore, the state space model is:

$$\begin{bmatrix} \dot{x_1} \\ \dot{x_2} \end{bmatrix} = \begin{bmatrix} 0 & 1 \\ \frac{-k}{m} & \frac{-b}{m} \end{bmatrix} \begin{bmatrix} x_1 \\ x_2 \end{bmatrix} + \begin{bmatrix} 0 \\ \frac{1}{m} \end{bmatrix} u + \begin{bmatrix} 0 \\ \frac{1}{m} \end{bmatrix} w \tag{3.42}$$

Where x_1 and x_2 is the is the position and velocity respectively. Table 3.2 below show the parameters:

Table 3.1 Parameters of the MSD system

Parameters	Symbol	Values
Mass	m	1 kg
Spring Coefficient	k	2 N/m
Damping Coefficient	b	3 N·s/m

Figure 3.5 below shows the disturbance input force acting on the MSD:

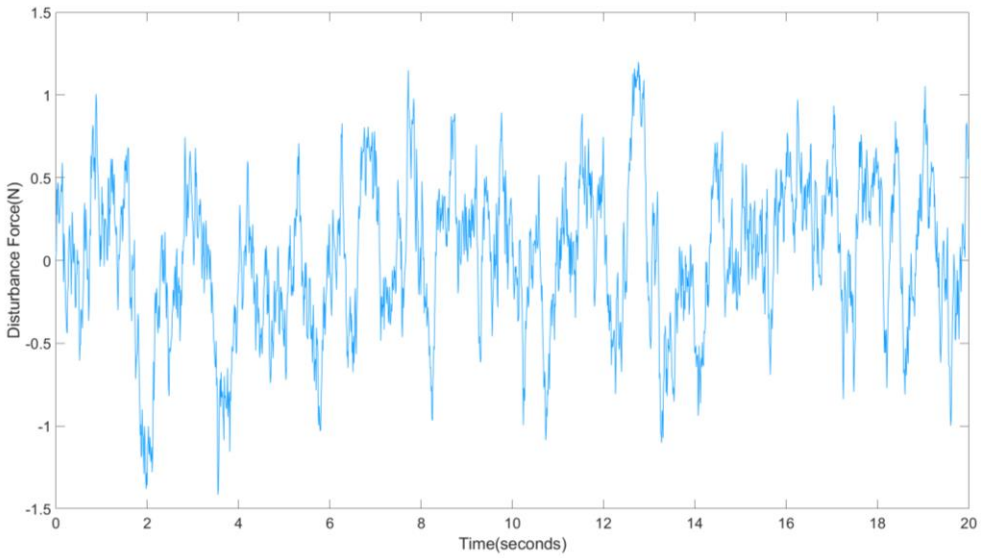

Figure 3.5 Disturbance force applied on the MSD system

The objective of the controller is to make sure the MSD system follows reference position. The design parameters will be configured to prioritize this position, as shown:

$$\boldsymbol{H_{11}} = \begin{bmatrix} 10 & 0 & 0 \\ 0 & .1 & 0 \\ 0 & 0 & 3 \end{bmatrix}, \boldsymbol{H_{12}^T} = \boldsymbol{H_{21}} = [0 \quad 0 \quad 0 \quad 0]$$

The sliding gain will be $\eta = 3$. Once the control gain (R) is selected, Eqs. (3.25) needs to be minimized iteratively to obtain the sliding mode gains, as shown in Figure 3.6 below:

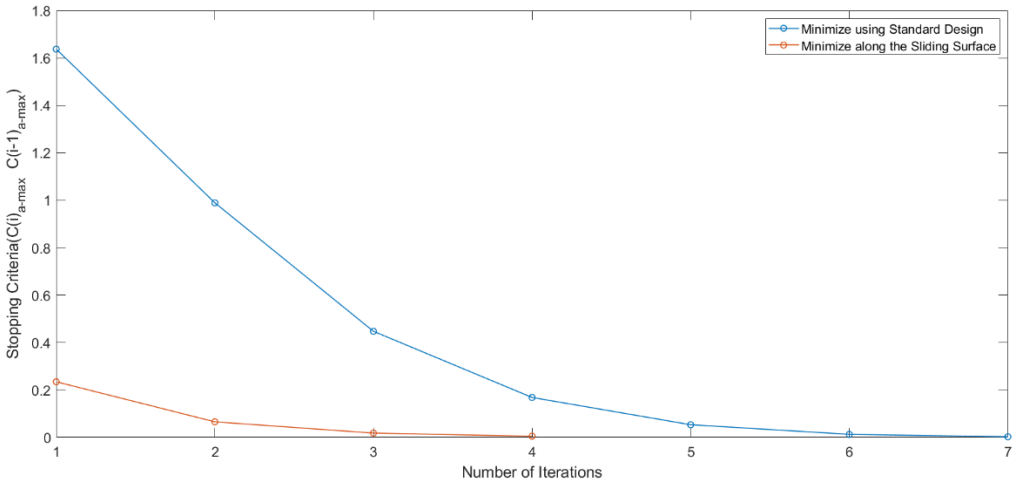

Figure 3.6 Example of the error being minimized with R = 1

Figure 3.7 and Table 3.2 below the results using Standard design parameters:

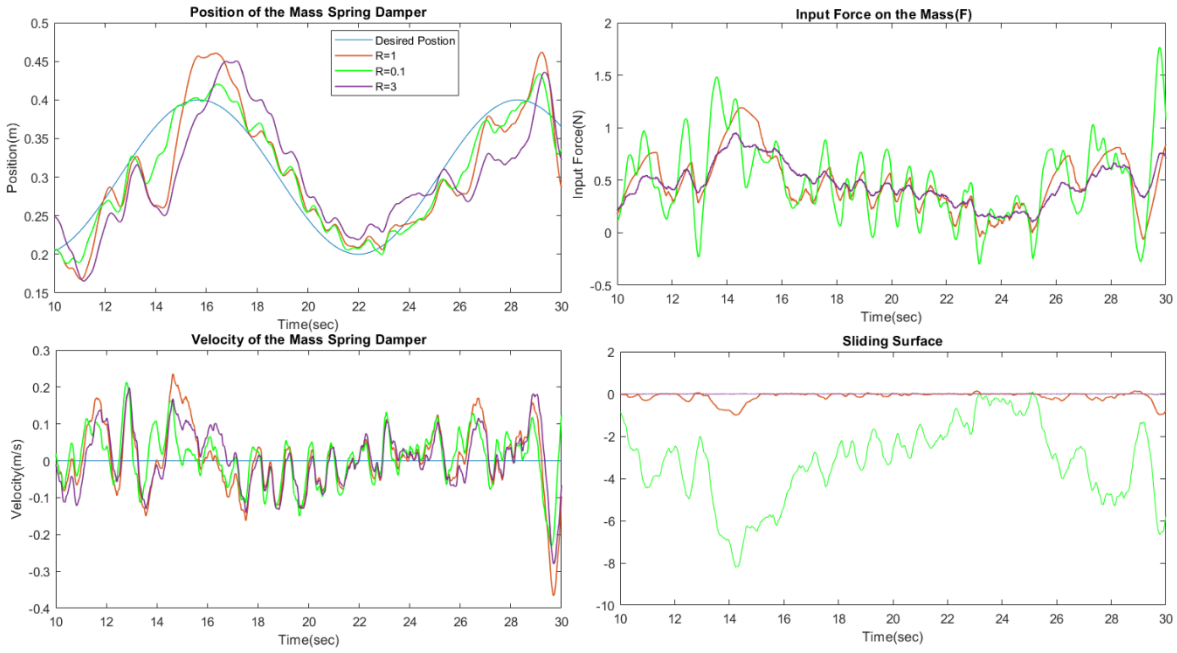

Figure 3.7 Results of using the FODSMCI as the controller using standard design parameters on the MSD

Table 3.2 MSD Error for 40 seconds with difference Penalties using standard design parameters

Parameters	**RSME of the Position**
$\boldsymbol{R = 0.1}$	2.9%
$\boldsymbol{R = 0.5}$	3.1%
$\boldsymbol{R = 1}$	5.4%
$\boldsymbol{R = 3}$	6.9%
$\boldsymbol{R = 5}$	8.6%

Figure 3.8 and Table 3.3 below show the results using the sliding gains ($\boldsymbol{C_a}$) minimizing the cost function along the sliding surface ($\boldsymbol{H_{11} = C_a^T C_a}$):

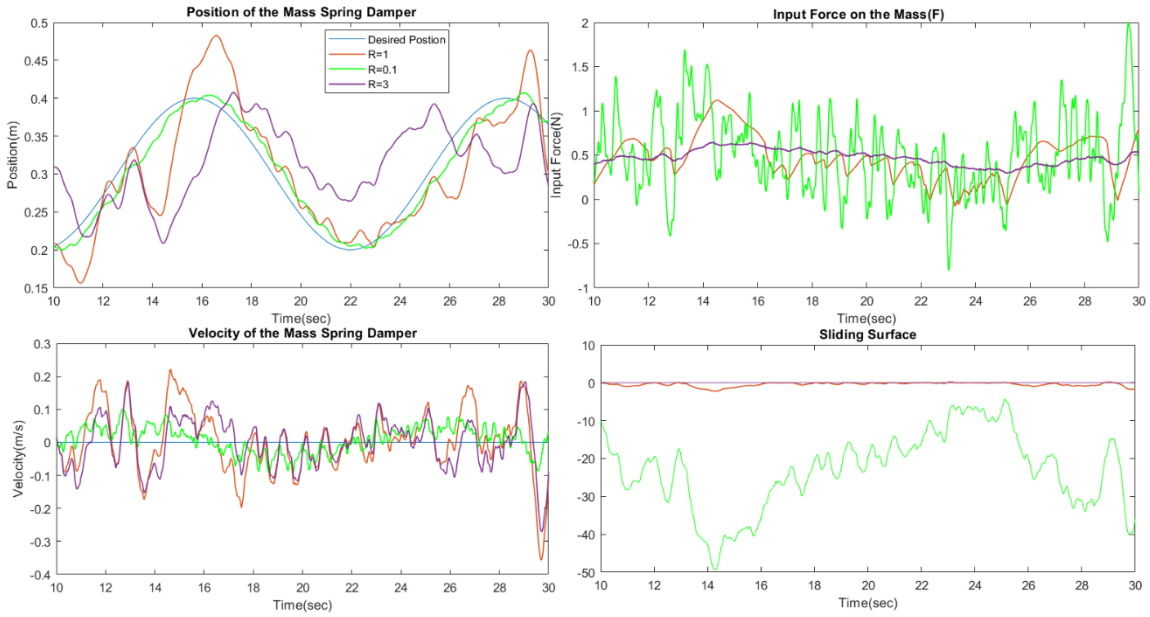

Figure 3.8 Results of using the FODSMCI as the controller using $\boldsymbol{H_{11} = C_a^T C_a}$ on the MSD

Table 3.3 MSD Error for 40 seconds with difference Penalties using $\boldsymbol{H_{11} = C_a^T C_a}$

Parameters	**RSME of the Position**
$\boldsymbol{R = 0.1}$	1.8%
$\boldsymbol{R = 0.5}$	2.9%
$\boldsymbol{R = 1}$	6.3%
$\boldsymbol{R = 3}$	9.5%
$\boldsymbol{R = 5}$	16.8%

In Figure 3.6 and 3.7, it could be observed that the FODSMCI applied a filtering mechanism to the error signal before transmitting it to the input force. This filtering action contributed to achieving a smooth response from the controller without exhibiting chattering behavior. Analyzing the results obtained from both methods of minimizing the cost function, as depicted in Table 3.2 and 3.3, it was noticeable that increasing the parameter R enhanced the controller's performance in terms of smoothness. However, a trade-off was observed, as the position tracking ability deteriorated with higher values of R. Conversely, when R was

decreased, the controller became more aggressive, leading to an improvement in position tracking.

The process shown in this section will be similar when testing the wind turbine models and evaluating the controller's performance.

3.4 Wind Turbine Models

This section will go over the Wind Turbine models used to test the novel reference tracker and controller.

3.4.1 Dynamic Modelling of the System of the Simple Wind Turbine

This Simple Wind Turbine (SWT) model was developed as it provides a useful starting point for understanding the fundamental behavior of a wind turbine, it should be noted that it represents an idealized case and does not fully representative of a real-world system. Real-world wind turbines are subject to various environmental factors such as wind speed, direction and turbulence that could affect the performance, safety, and energy production of the turbine. Other factors such as the materials used for the turbine's construction and the control system design may also introduce deviation from the ideal model.

It should be noted that the model represents an idealized scenario and may not accurately reflect a real-world system. The wind turbine model was created using the dynamic equations of a two mass system as shown in Figure 3.9 below:

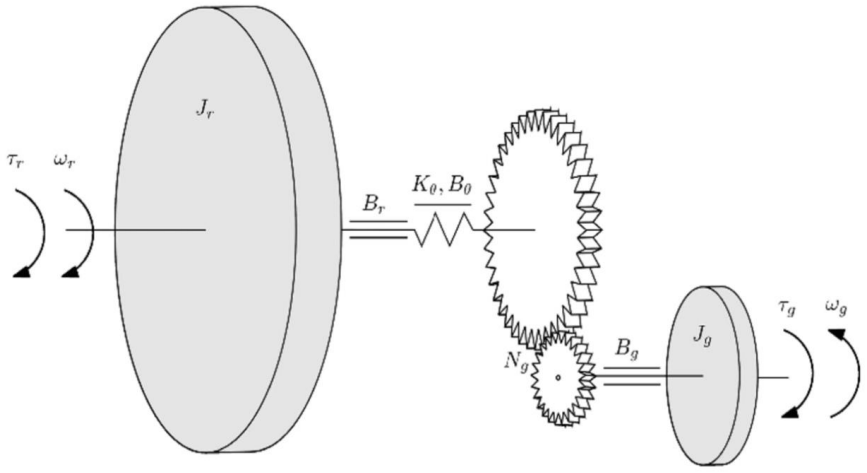

Figure 3.9 Model of a wind turbine drivetrain system

Table 3.4 give the values and description of each component. The differential equation of Figure 3.9 above can be derived using Newtons second law:

$$J_r\dot{\omega}_r = \tau_r - K_\theta\theta - (B_\theta + B_r)\omega_r + \frac{B_\theta}{N_g}\omega_g \tag{3.43}$$

$$J_g\dot{\omega}_g = \frac{K_\theta}{N_g}\theta + \frac{B_\theta}{N_g}\omega_r - \left(\frac{B_\theta}{N_g^2} + B_g\right)\omega_g - \tau_g \tag{3.44}$$

$$\dot{\theta} = \omega_r - \frac{1}{N_g}\omega_g \tag{3.45}$$

Eqs. (3.43) to (3.45) can be rearranged to find the first order state space of the system. This derivation is based on Soltani et al. [45] and Bianchi et al. [7]:

$$\begin{bmatrix}\dot{\omega}_r \\ \dot{\omega}_g \\ \dot{\theta}\end{bmatrix} = \begin{bmatrix}\frac{-B_d}{J_r} & \frac{B_d}{NJ_r} & \frac{-K_d}{J_r} \\ \frac{B_d}{NJ_g} & \frac{-B_d}{N^2J_g} & \frac{K_d}{NJ_g} \\ 1 & \frac{-1}{N} & 0\end{bmatrix}\begin{bmatrix}\omega_r \\ \omega_g \\ \theta\end{bmatrix} + \begin{bmatrix}0 \\ \frac{-1}{J_g} \\ 0\end{bmatrix}[T_g] + \begin{bmatrix}\frac{1}{J_r} \\ 0 \\ 0\end{bmatrix}[T_r] \tag{3.46}$$

$$\dot{x} = \boldsymbol{A}x + \boldsymbol{B_c}u + \boldsymbol{B_d}d \tag{3.47}$$

Where $x \in R^n, u \in R$ and $d \in R$, are the wind turbine state, generator input torque (T_g) as input and rotor aerodynamic torque (T_r) as disturbance. $\boldsymbol{A}$, $\boldsymbol{B_c}$, and $\boldsymbol{B_d}$ are the state, control, and disturbance matrix. ω_r denotes the rotor speed, ω_g denotes the generator speed, and θ denotes the torsion angle of the drivetrain.

The rotor aerodynamic torque (T_r) is the torque generated by the wind turbine rotor blades as they extract energy from the wind. T_r is a function of the wind speed, tip speed ratio and power coefficient, defined as:

$$T_r = \frac{1}{2}\rho\pi R^3\frac{C_p(\lambda,\beta)}{\lambda}V^2 \tag{3.48}$$

The aerodynamic power coefficient (C_p) measures the power that the wind turbine extracts from the wind, it is the ratio of generated power to total power in the wind passing through the rotor.

While aerodynamic power is dependent on the tip speed ratio (λ) and pitch angle (β), in real life it is dependent on the geometry of the rotor blades, air density and wind direction. Even things like ice and dirt building up on the blades as well as erosions of the blades will affect the power captured by the blades as it affects its geometry. However, this section will only focus on the making the C_p dependent on the tip speed ratio (λ) and pitch angle (β).

Therefore, different techniques like exponential, sinusoidal, polynomial, or data-driven algorithms [46] can be used to model C_p. However, for this paper, this specific model will be used:

$$C_{\mathrm{p}}(\lambda,\beta) = 0.5176\left(\frac{116}{\lambda_i} - 0.4\beta - 5\right)\mathrm{e}^{\frac{-21}{\lambda_i}} + 0.0068\lambda$$
$$\frac{1}{\lambda_i} = \frac{1}{\lambda + 0.08\beta} - \frac{0.035}{\beta^3 + 1} \tag{3.49}$$

Table 3.4 below shows the wind turbine characteristics to develop the wind turbine model for simulation. These parameters are based on the 5MW onshore horizontal wind turbine [47]. Therefore, the rated power of the turbine will be 5MW.

Table 3.4 Wind Turbine Parameters used in Simulation for a 5MW wind turbine.

Symbol	Description	Value
B_d	Drivetrain damping coefficient	$6.215\mathrm{E}6\,\frac{\mathrm{Nms}}{rad}$
K_d	Drivetrain spring constant	$8.68\mathrm{E}8\,\frac{\mathrm{Nm}}{\mathrm{rad}}$
J_r	Rotor inertia	$38677056\ \mathrm{kg\ m^2}$
J_g	Generator inertia	$534.1\ \mathrm{kgm^2}$
N	Gearbox ratio	97
R	Rotor blade radius	63 m
ρ	Air density	$1.225\,\frac{\mathrm{kg}}{\mathrm{m}^3}$

Figure 3.10 below shows how the wind turbine system will be designed in Simulink. The generator torque will be used as the control input to make sure the rotor speed tracks the optimal

rotor speed. The aerodynamic rotor torque is a function of the rotor speed, wind speed and power coefficient and will be used as the disturbance input. This thesis will not incorporate pitch control to maximize power and will maintain the pitch at 0°.

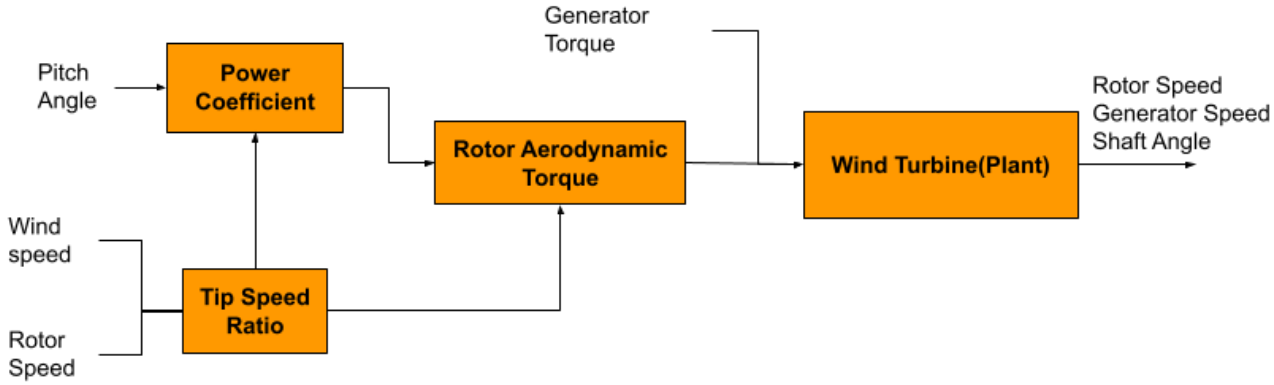

Figure 3.10 Overview of the SWT

3.4.2 Validating results using FAST

FAST (Fatigue, Aerodynamics, Structures, and Turbulence) [16] is a wind turbine simulation software developed by the National Renewable Energy Laboratory (NREL) in the United States. It is a comprehensive tool for simulating the behavior of wind turbines under various operating conditions. The software can model wind turbines of different sizes and designs, including both fixed and variable speed turbines. It simulates the turbine's dynamics, encompassing blade aerodynamics, mechanical and electrical systems, and the interaction between the turbine and surrounding wind and terrain.

An interface has been developed to integrate FAST with Simulink. This will allow the user to implement advanced turbine controls using Simulink's block diagrams. FAST supports five fundamental control methods: blade pitching, generator torque control, high-speed shaft braking, tip brake deployment, and nacelle yawing. In the context of this thesis, only generator torque control will be utilized.

The wind turbine model utilized in this study is based on the design proposed by Jonkman [10]. This allows for the utilization of certification tests to evaluate the performance of the

turbine. The turbine in question is an onshore model, featuring three blades and having a rated capacity of 5MW.

3.5 Wind generation

To evaluate the model effectively, real-world wind data should be incorporated, and therefore TurbSim (Turbulence Simulator) [48] will be employed. Developed by the NREL, TurbSim is a simulation software designed to model the time-varying characteristics of wind flow, such as wind speed and turbulence, at a wind turbine's hub height. By utilizing a stochastic model, TurbSim generates a time series of wind data based on the statistical analysis of measured or simulated wind data. This output can then be fed into the wind turbine simulator, enabling the analysis of wind turbine performance and behavior under various wind conditions.

Chapter 4 Implementation of Methods

In this section, the techniques outlined in Chapter 3 will be examined. The presentation and assessment of the reference tracking and controller outcomes will be conducted by applying them to both the SWT and FAST models.

4.1 Wind generation and noise filtering

The simulations utilize wind inputs generated by TurbSim, consisting of 31 x 31 grids of IEC Class B Kaimal-spectrum turbulence, with samples taken every 50 milliseconds. Each simulation has a duration of 500 seconds, but the results are computed based on the final 400 seconds in order to mitigate the influence of initial conditions. Additionally, the mean wind speed for these simulations is set at 5 m/s.

The wind data is first filtered through a low-pass filter (Eqs. (4.1)) before entering the controller, as depicted in Figure 4.1. This filter effectively reduces high-frequency noise, which in turn enhances the performance of the control system.

$$H(s) = \frac{1}{\frac{1}{\omega_c}s + 1} \tag{4.1}$$

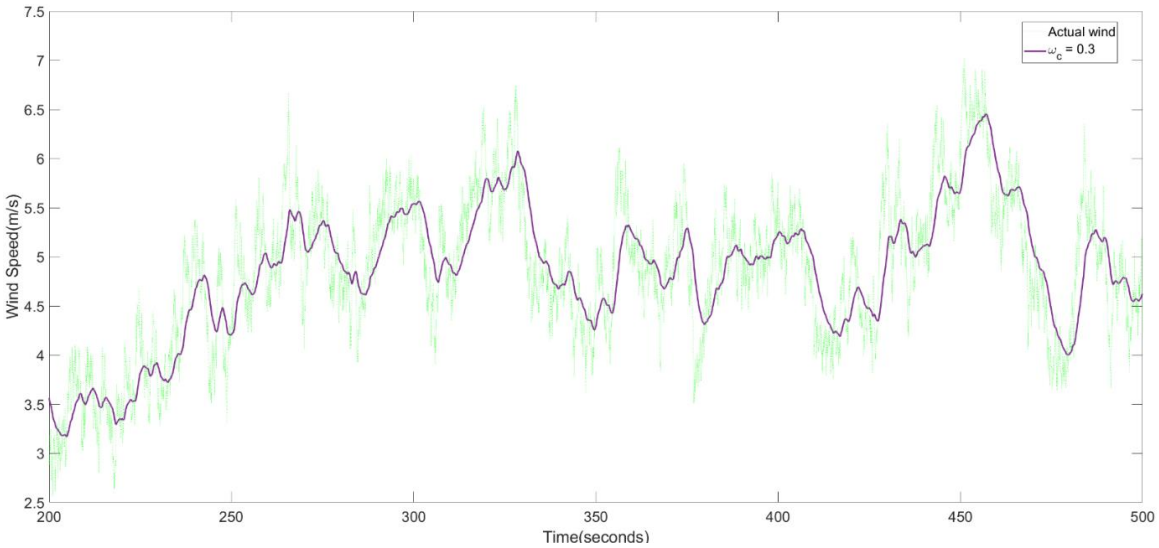

Figure 4.1 Wind Speed Profile with Turbulence to be used a disturbance input for the aerodynamic rotor torque

A low pass filter was chosen for its simplicity and ease of tuning, making it an optimal choice considering the thesis' focus on turbine control, where implementing a complex filter was deemed unnecessary. By removing rapid fluctuations, the filter enables the steady-state wind to be accurately analyzed by the controller. The selection of the cut-off frequency (ω_c) needs to aim to strike a balance between the fidelity of the wind signal and noise removal. A lower ω_c provides a cleaner signal but risks filtering out important information. A higher ω_c might retain more noise, compromising accuracy. Therefore, $\omega_c = 0.3$ was carefully chosen for our purposes as it strikes a balance between accurately capturing the pertinent wind data and effectively filtering out unwanted noise.

Filtering the wind before it enters the control system is crucial, as unfiltered wind can cause mechanical stress and damage to critical components such as gearboxes, bearings, and blades. High-frequency noise and vibration present in unfiltered wind can also disrupt control signals, leading to unstable operation and reduced power output. By filtering the wind, these disturbances are smoothed out, resulting in improved accuracy and stability of the turbine control system.

Furthermore, wind filtering is necessary to protect not only the turbine components but also the sensors, actuators, and control electronics. Wind turbine control systems are sensitive to high-frequency noise, which can interfere with control signals and generate inaccurate readings. Therefore, filtering the wind before it enters the control system is essential for ensuring the reliability and optimal performance of wind turbines.

4.2 Recursive least squares with a forgetting factor as the reference tracker

The method outlined in Section 3.1 was used to find the optimal TSR. To simulate the change in optimal TSR, the turbine characteristics will change after 350 seconds. A sample period of $T_s = 0.5$ seconds was also selected, as it strikes a balance between capturing rapid changes in the system dynamics and minimizing the computational load in real-time applications. This time interval ensures that important data points are captured frequently enough to maintain accuracy and responsiveness. However, it is essential to consider that in real-world

applications, such as monitoring a turbine that operates for a prolonged period, a sample rate of 0.5 seconds may be too fast.

In this section, the RLS reference tracker will be tested using different forgetting factors on the SWT and FAST to determine the optimal TSR that will keep the turbine at the MPP.

4.2.1 Results using the RLS with a forgetting factor on the SWT

In order to evaluate the performance of the proposed control method, we will use the TSR as an input and the rotor power coefficient as the output. After 350 seconds, the optimal TSR of the aerodynamic power coefficient (as described by Eqs. (3.49)) is altered to simulate the effects of dirt or snow accumulation on the wind turbine. Figure 4.2 below illustrates that the RLS method successfully tracks the optimal TSR. By incorporating a high forgetting factor (μ), the system can respond more rapidly to changes.

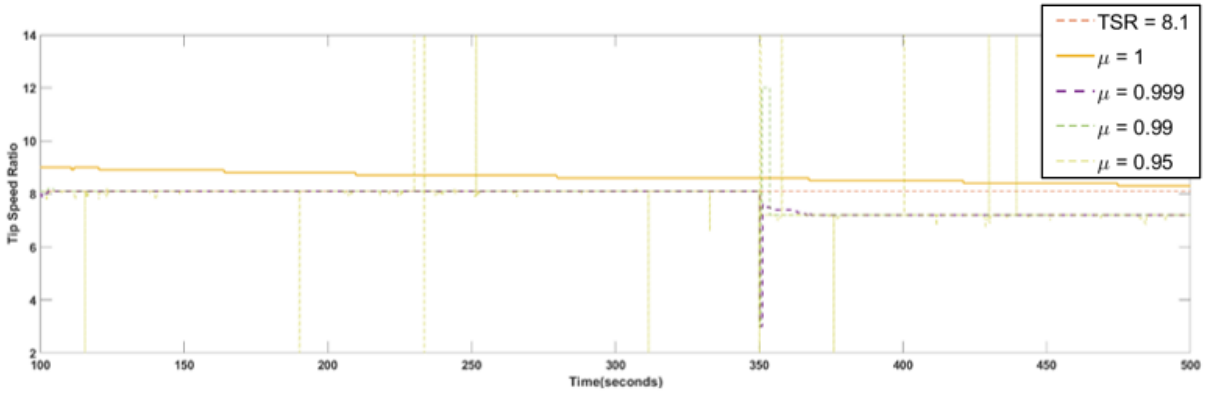

Figure 4.2 Optimal TSR using RLS with a forgetting factor for the SWT

Table 4.1 Power generated using the RLS with different forgetting factors on the SWT for 200 seconds

Parameters	Energy Generated (MJ)	% Change from the Optimal TSR
$\boldsymbol{TSR = 8.1}$	101.7	-
$\boldsymbol{\mu = 1}$	100.4	-1.3%
$\boldsymbol{\mu = 0.999}$	104.3	2.5%
$\boldsymbol{\mu = 0.99}$	105.1	3.3%

$\boldsymbol{\mu = 0.95}$	102.5	0.8%
$\boldsymbol{\mu = 0.90}$	99.5	-3.2%
$\boldsymbol{\mu = 0.85}$	89.5	-12.9%

As demonstrated by from Figure 4.2 and Table 4.1, the Recursive RLS method is effective in tracking the optimal TSR for the SWT model. When the ideal TSR is fixed, it generates less power since it is not at the optimal point when the turbine characteristics change. This highlights the need for a reference tracker to ensure the wind turbine operates at maximum efficiency. In situations where there is no forgetting factor ($\mu = 1$), the RLS method takes time to find the optimal TSR, as it is heavily influenced by past data. In contrast, introducing a forgetting factor allows the system to adapt more efficiently. However, it is crucial to maintain a high forgetting factor, as a low one can result in system instability.

It is important to note that the system performs optimally with a low forgetting factor, but this is not a significant concern since wind turbine characteristics change gradually rather than abruptly. Thus, utilizing a higher forgetting factor enables the system to better adapt to these changes, ultimately leading to improved performance.

4.2.2 Results using the RLS with a forgetting factor using FAST

This section will test the RLS method with the Forgetting Factor using FAST. Figure 4.3 and Table 4.3 below shows the results:

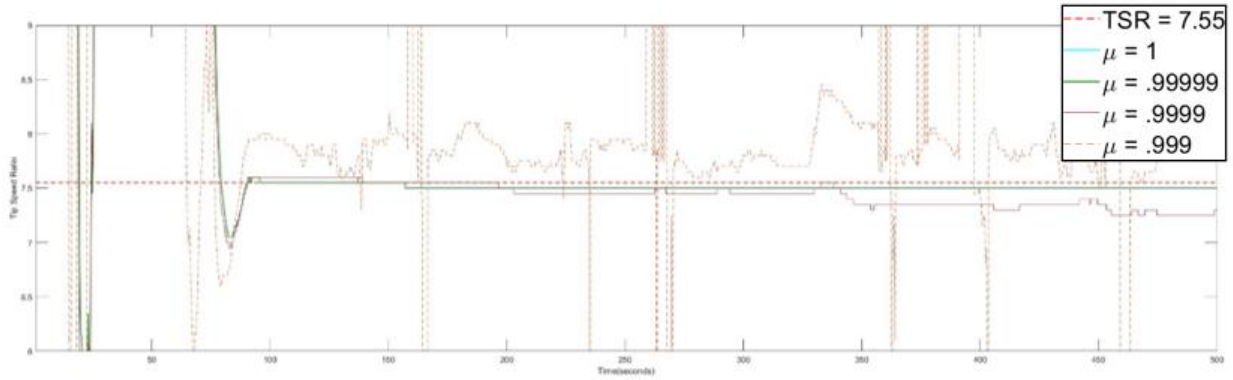

Figure 4.3 Optimal TSR using RLS with a forgetting factor on FAST

Table 4.2 Power generated using the RLS with different forgetting factors using FAST for 200 seconds

Parameters	Energy Generated (MJ)	% Change from Theoretical TSR
$\boldsymbol{TSR = 7.55}$	100.62	-
$\boldsymbol{\mu = 1}$	100.57	0.0%
$\boldsymbol{\mu = 0.99999}$	100.66	0.0%
$\boldsymbol{\mu = 0.9999}$	100.78	0.2%
$\boldsymbol{\mu = 0.999}$	98.43	-2.2%
$\boldsymbol{\mu = 0.99}$	81.26	-19.2%

Figure 4.3 above demonstrates the results obtained when testing with the RLS using the FAST model. These results align closely with those obtained by the SWT, showing that the RLS algorithm has the capability to effectively track the optimal TSR. Despite this, it's necessary to highlight that the RLS method requires a particularly high forgetting factor to maintain tracking accuracy. As illustrated in Table 4.2, as μ decreases, a slight improvement becomes noticeable. However, once $\mu = 0.999$, the tracker starts to lose stability and becomes less effective at tracking the optimal TSR.

4.3 First Order Dynamic SMC with Integration as the Controller

The FODSMCI offers flexibility in the design of sliding surfaces and closed-loop dynamics to achieve specific performance objectives. In particular, the aim is to balance the conflicting goals of maximizing power generation and extending the life of the wind turbine. Two design parameters will be considered when minimizing the cost function (Eqs. (3.25)). The first one is using standard design parameters are used as shown below:

$$\boldsymbol{H_{11}} = \begin{bmatrix} 10 & 0 & 0 & 0 \\ 0 & .01 & 0 & 0 \\ 0 & 0 & .01 & 0 \\ 0 & 0 & 0 & H_{11}(4,4) \end{bmatrix}, \boldsymbol{H_{12}^T = H_{21}} = [0 \quad 0 \quad 0 \quad 0.1]$$

The other design parameter will minimize the cost function along the sliding surface ($\boldsymbol{H_{11} = C_a^T C_a}$) as shown in Section 3.2.2.

The focus of this thesis is to optimize the power generated by the wind turbine. To do this, the controller is designed to make sure that the system consistently operates at its maximum power point. A crucial aspect of this process is the regulation of rotor speed to align with the desired rotor speed determined in section 4.2, hence $\boldsymbol{H_{11}}(1,1) = 10$. Also, as mentioned in the Section 3.2, only adjusting the generator torque will be used to control the turbine. This section will discuss the utilization of different penalty gains (R) and show casing the results.

4.3.1 Results of using the FODSMCI to control the SWT

This section will present the outcomes of employing FODSMCI as the controller, tested on the (SWT). Figure 4.4, 4.5 and Table 4.3 below show the results using Standard design parameters.

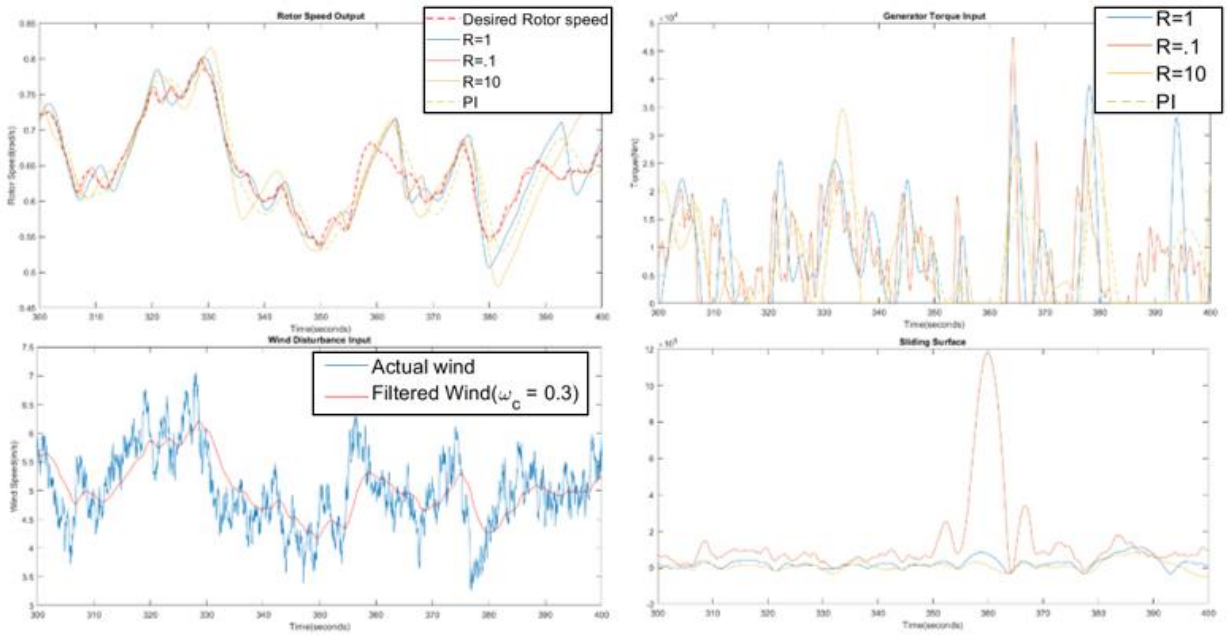

Figure 4.4 Results of FODSMCI with different penalties using standard design parameters on the SWT

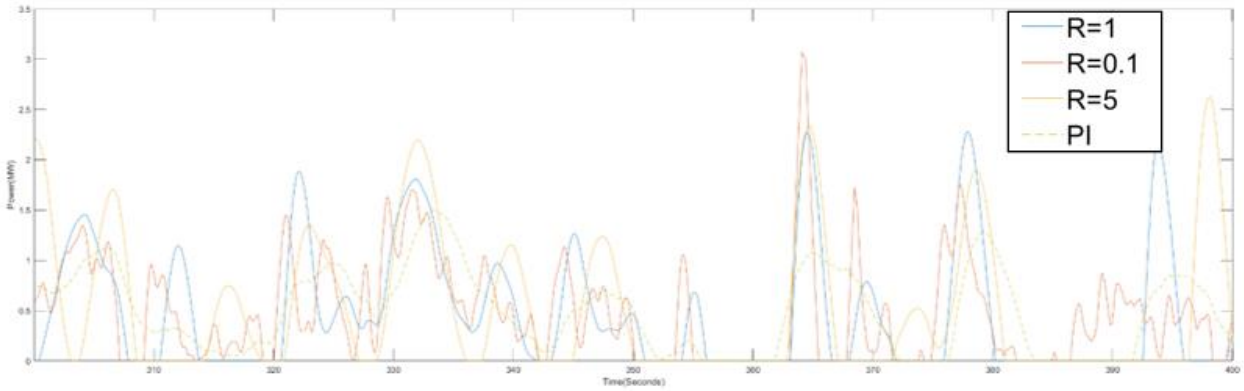

Figure 4.5 Power Generated over time compared with different penalties using standard design parameters on the SWT

Table 4.3 Results for 200 seconds with difference Penalties using standard design parameters the SWT

Parameters	Energy Generated (MJ)	% Change from R=1	RMSE of the Rotor Speed
$\boldsymbol{R = 0.01, H_{11}(4,4) = 1}$	100.49	-1.2%	5.3%
$\boldsymbol{R = 0.1, H_{11}(4,4) = 1}$	102.11	0.4%	2.0%
$\boldsymbol{R = 1, H_{11}(4,4) = 1}$	101.77	-	4.1%
$\boldsymbol{R = 5, H_{11}(4,4) = 3}$	99.50	-2.2%	3.6%
$\boldsymbol{R = 10, H_{11}(4,4) = 3}$	83.76	-17.7%	10.9%
$\boldsymbol{PI}$	99.91	-2.7%	3.2%

As seen from Figure 4.4 and 4.5. above ,the FODSMCI effectively filters the error signal before it is sent to the generator, resulting in a smooth response without chattering, eliminating the need for boundary layers. The results shown in Table 4.3, along with the accompanying figures, demonstrate how adjusting the Control Gain (R) affects power generation and the accuracy of rotor speed tracking, as calculated using the Root Mean Square Error (RMSE). When R is increased, it places greater emphasis on minimizing control effort, which in turn gives rise to a more conservative controller that consumes less energy. This augmentation in R also induces a notable enhancement in the controller's operational smoothness. However, this advantage is counterbalanced by a corresponding deterioration in rotor speed tracking, resulting

in diminished energy production. Such deterioration can further compromise the overall tracking performance, potentially leading to underperformance of the wind turbine. Also, If the control penalty gain is set exceedingly high, the controller becomes overly cautious in applying control effort. This conservative approach makes it overlook the state error, causing a substantial deviation from the desired output. To counterbalance this effect for higher R, an increase in the integral gain ($\boldsymbol{H_{11}}(4,4)$) becomes necessary. This adjustment helps to compensate for the overly cautious controller and allows it to maintain its operation effectively.

In contrast, decreasing the R puts less emphasis on minimizing control effort, which leads the controller to adopt a more aggressive stance in adjusting generator torque. This change consequently results in improved rotor speed performance. However, this improvement is not without its drawbacks, primarily manifesting as increased oscillations in the generator torque. This phenomenon is driven by an inherent need to minimize the error. While these adjustments do enhance tracking performance and potentially boost power output, they carry the risk of necessitating higher control effort and potentially inducing mechanical stress. If the Control Penalty Gain is set too low, it could result in controller overcompensation. Although this scenario might improve rotor speed tracking, the power generated could be reduced due to the overcompensation and added strain on the generator.

Figure 4.6, 4.7 and Table 4.4 below show the results using the sliding gains ($\boldsymbol{C_a}$) minimizing the cost function along the sliding surface ($\boldsymbol{H_{11} = C_a^T C_a}$):

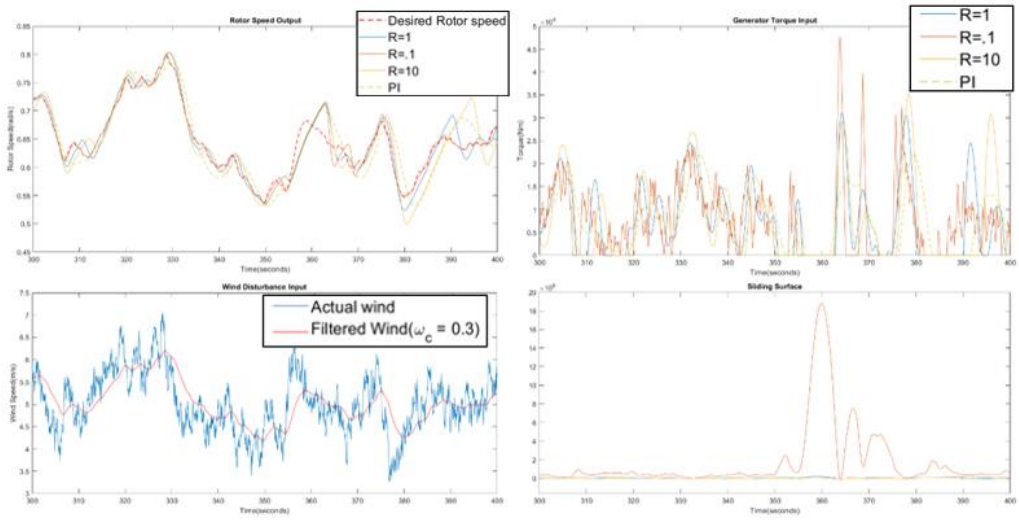

Figure 4.6 Results of FODSMCI with different penalties with using $\boldsymbol{H_{11} = C_a^T C_a}$ on SWT

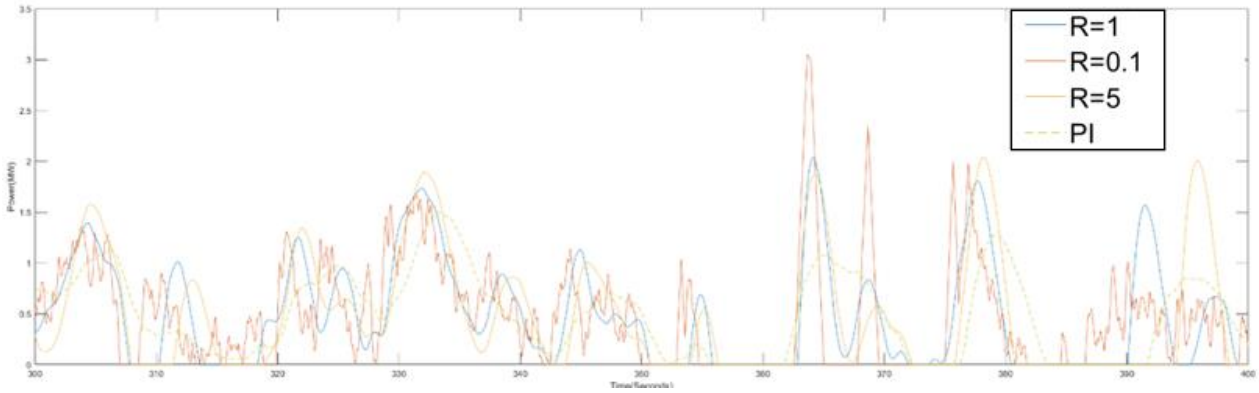

Figure 4.7 Results of FODSMCI with different penalties with using $\boldsymbol{H_{11} = C_a^T C_a}$ on SWT

Table 4.4 Power generated for 200 seconds with difference Penalties using $\boldsymbol{H_{11} = C_a^T C_a}$ on SWT

Parameters	Energy Generated (MJ)	% Change from R=1	RMSE of the Rotor Speed
$\boldsymbol{R = 0.01, H_{11}(4,4) = 1}$	101.50	-1.2%	5.6%
$\boldsymbol{R = 0.1, H_{11}(4,4) = 1}$	103.10	0.4%	1.1%
$\boldsymbol{R = 1, H_{11}(4,4) = 1}$	102.71	-	2.6%
$\boldsymbol{R = 5, H_{11}(4,4) = 3}$	98.51	-4.1%	6.2%
$\boldsymbol{R = 10, H_{11}(4,4) = 3}$	83.85	-18.4%	19.0%
$\boldsymbol{PI}$	99.91	-2.7%	3.2%

Comparing the of two different design parameters aimed at reducing the cost function, the standard design methods perform somewhat worse than when $\boldsymbol{H_{11} = C_a^T C_a}$. These differences can be attributed to the reduction of the cost function along the sliding surface, which appears to yield small but improved result, especially when the control is not penalized. These findings highlight a trade-off between the smoothness of controller performance and rotor speed tracking. This trade-off suggests that optimizing one aspect may compromise the other, indicating a balancing act in controller design that must carefully consider the desired outcome versus the potential costs in performance.

4.3.2 Results of using the FODSMCI to control the turbine in FAST for Validation

To validate the controller, this section will present the outcomes of employing FODSMCI as the controller, tested on FAST model. Figure 4.8, 4.9 and Table 4.5 below show the results using standard design parameters:

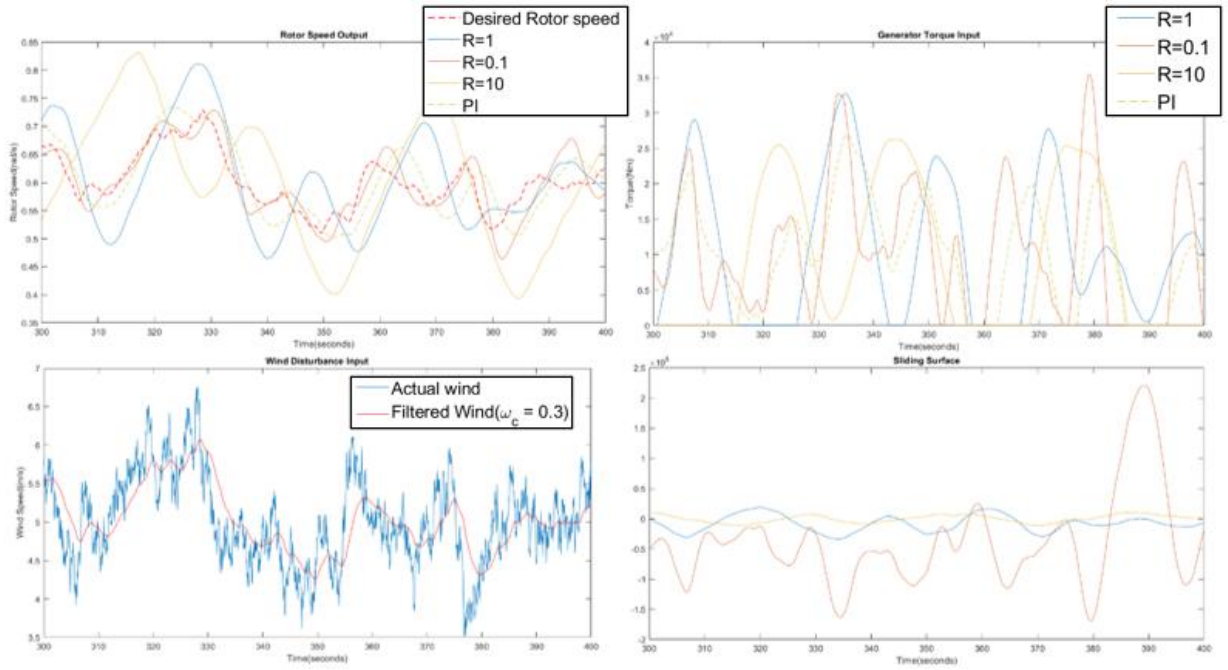

Figure 4.8 Results of FODSMCI with different penalties using standard design parameters on the FAST simulator

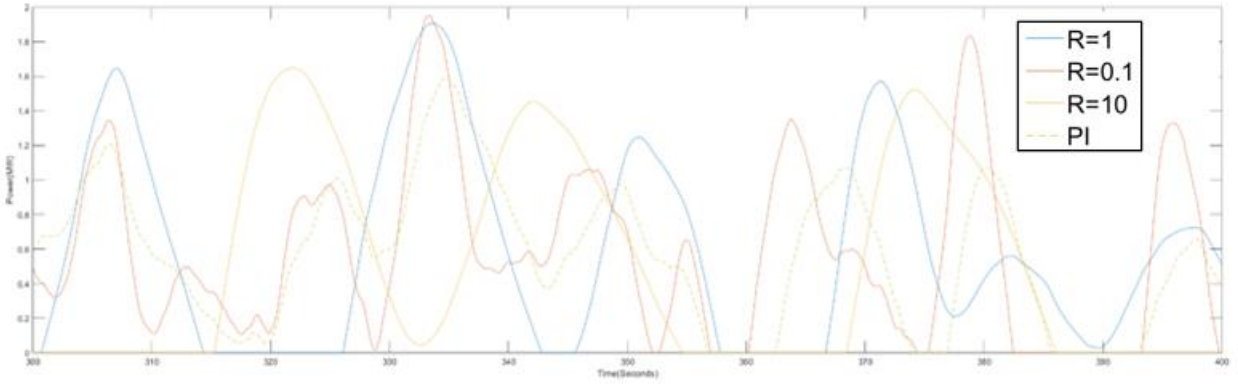

Figure 4.9 Power Generated over time compared with different penalties using standard design parameters on the FAST simulator

Table 4.5 Power generated for 200 seconds with difference Penalties using standard design parameters on FAST

Parameters	Energy Generated (MJ)	% Change from R=1	RMSE of the Rotor Speed
$\boldsymbol{R = 0.01, H_{11}(4,4) = 1}$	105.08	4.0%	2.4%
$\boldsymbol{R = 0.05, H_{11}(4,4) = 1}$	105.72	2.6%	3.1%
$\boldsymbol{R = 0.1, H_{11}(4,4) = 1}$	106.32	3.2%	3.8%
$\boldsymbol{R = 1, H_{11}(4,4) = 1}$	103.01	-	6.3%
$\boldsymbol{R = 10, H_{11}(4,4) = 50}$	101.01	-1.9%	7.2%
$\boldsymbol{R = 30, H_{11}(4,4) = 50}$	99.50	-3.4%	8.5%
$\boldsymbol{PI}$	105.31	2.2%	4.2%

Observing Figure 4.8 and 4.9, the FODSMCI results tested on FAST align with the results found in the SWT (Section 4.3.1). The controller effectively filters the error signal before sending it to the generator, producing a smooth response without chattering. Reviewing the figures and Table 4.5, an increase in Control Penalty Gain (R) puts more emphasis on minimizing control effort. However, increasing R also results in deteriorating rotor speed tracking as the controller becomes overly cautious in applying control effort, even though it improves the controller's smoothness. Conversely, as R decreases, the controller becomes more aggressive, leading to improved rotor speed performance.

Figure 4.10 and 4.11 and Table 4.6 below show the results using the sliding gains ($\boldsymbol{C_a}$) minimizing the cost function along the sliding surface ($\boldsymbol{H_{11} = C_a^T C_a}$):

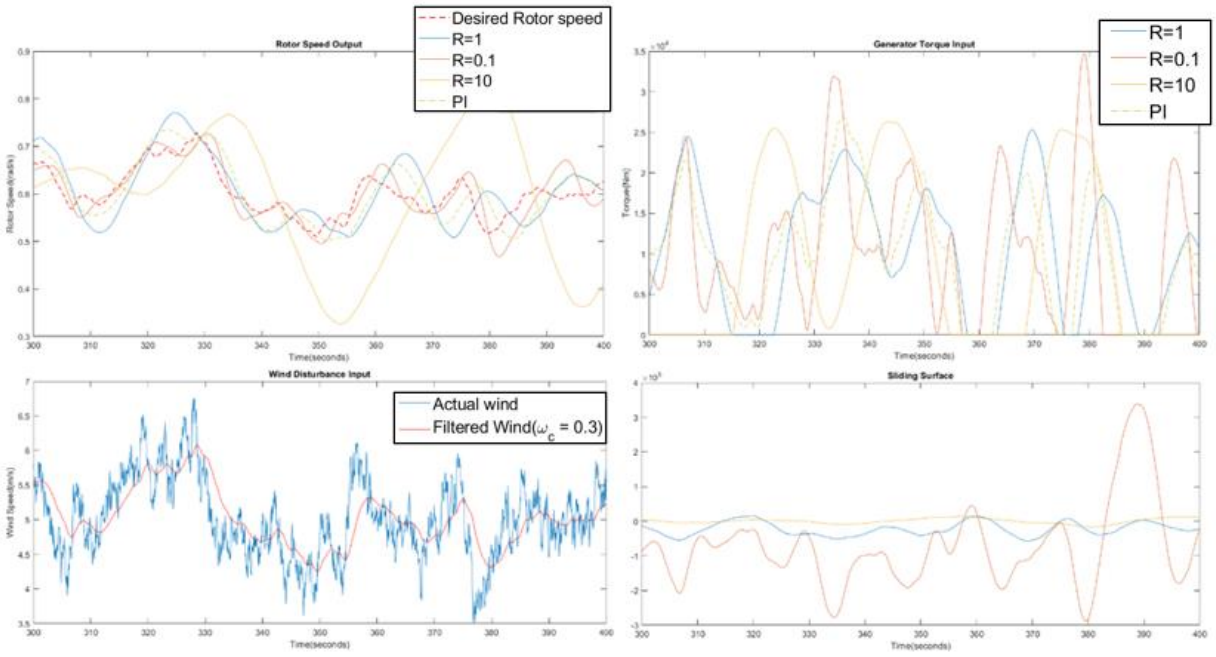

Figure 4.10 Results of FODSMCI with different penalties with using $\boldsymbol{H_{11} = C_a^T C_a}$ on the FAST simulator

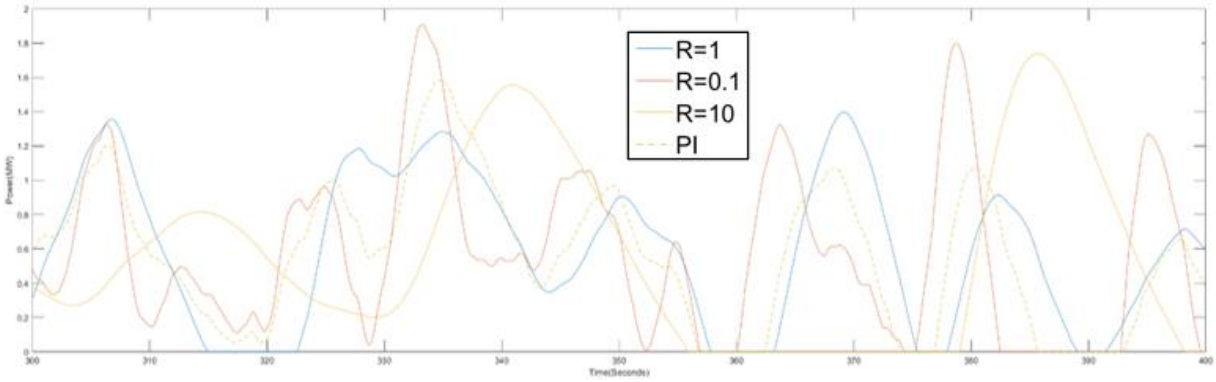

Figure 4.11 Power Generated over time compared with different penalties with using $\boldsymbol{H_{11} = C_a^T C_a}$ on the FAST simulator

Table 4.6 Power generated for 200 seconds using $\boldsymbol{H_{11} = C_a^T C_a}$ on FAST

Parameters	Energy Generated (MJ)	% Change from R=1	RMSE of the Rotor Speed
$\boldsymbol{R = 0.01, H_{11}(4,4) = 1}$	104.76	3.1%	3.4%
$\boldsymbol{R = 0.05, H_{11}(4,4) = 1}$	105.68	3.7%	2.8%
$\boldsymbol{R = 0.1, H_{11}(4,4) = 1}$	107.10	5.4%	2.4%
$\boldsymbol{R = 1, H_{11}(4,4) = 1}$	101.61	-	5.7%
$\boldsymbol{R = 10, H_{11}(4,4) = 50}$	98.70	-2.9%	9.4%
$\boldsymbol{R = 30, H_{11}(4,4) = 50}$	98.18	-3.4%	12.2%
$\boldsymbol{PI}$	105.31	3.6%	4.2%

When comparing methods intended to reduce the cost function, the standard design methods somewhat underperform compared to when $\boldsymbol{H_{11} = C'C}$.

Comparing the results Section 4.3.1, it is evident that the RMSE of the rotor speed in the FAST Turbine Model is higher in comparison to the SWT model. The SWT model serves as a fundamental representation of a wind turbine system, merely encompassing basic dynamics. In contrast, the FAST Turbine Model constitutes a thorough simulation of wind turbine systems and is more adept at accurately portraying the non-linear dynamic response of a wind turbine. Additionally, if the control is excessively penalized on the FAST model, its energy generation diminishes, mirroring the consequences of such practices in actual wind turbines. The FAST model finds its greatest utility in regions with lower generation where the wind speeds range from 3-6 m/s.

Overall, the Simple 3rd Order Turbine System proves advantageous for initial control design and comprehension. Nevertheless, when it comes to the crucial task of validating control strategies before their actual deployment, more complex and detailed models like the FAST model are imperative. Thorough testing and evaluation are essential in ensuring the efficacy and reliability of control strategies in practical implementation.

Chapter 5 Summary and Suggestions

This section will provide a brief summary of the thesis and propose recommendations for future studies.

5.1 Summary of Thesis

This study aimed to enhance the power output of wind turbines by utilizing a reference tracker. This tracker helps determine the optimal point for maximizing power generation. Additionally, a controller was implemented to maintain the wind turbine's operation at this optimal point.

Chapter 1 provided an introductory overview of wind turbines, their operations, and associated methodologies. The initial discussion revolved around renewable energy, spotlighting the role that wind turbines play in this sector. The operational principles of wind turbines were then discussed, including their control strategies such as yaw, pitch, and generator torque control. The chapter further delved into the power regions of wind turbines, offering a succinct explanation of MPPT and power regulation regions. Lastly, underlying assumptions made throughout the study and an overarching summary of the thesis were provided, laying the groundwork for subsequent chapters.

Chapter 2 is a comprehensive review of various methodologies used in wind turbine operations. It covers different MPPT techniques, such as Perturb and Observe and Incremental Conductance, which were identified as essential for finding the optimal TSR. The chapter also discussed controller mechanisms including PID, LQR, and fuzzy logic, emphasizing their importance in ensuring optimal turbine operation. Additionally, the concept of SMC was introduced, with various SMC methods being examined for their potential to enhance the efficiency of wind turbines.

Chapter 3 focused on the development of various methods integral to the study. For the reference tracking method, a derivation using the Recursive Least Square with a forgetting factor was utilized. In terms of the controller, a strategy based on SMC was formulated. Specifically, the first order dynamic sliding mode control with integration was developed, ensuring that the system would operate at the optimal rotor speed. The chapter also featured the development of a

simplistic wind turbine model, which was used to test the model. Additionally, the chapter elucidated on the use of FAST, a tool developed by the NREL, employed to validate the model.

Chapter 4 presented the findings of the study. The chapter began by illustrating the wind generation process using Turbsim, highlighting how it was filtered using a first-order filter. The results from the reference tracking segment revealed the efficacy of the RLS with a forgetting factor in determining the optimal TSR. The forgetting factor enabled the reference tracker to identify the optimal TSR on the SWT. However, it was noted that the process was more challenging when using the FAST model. Additionally, the use of the FODSMCI exhibited certain trade-offs between controller performance and rotor speed tracking. Various control penalties were applied, and the outcomes were compared with the cost function minimized using standard design parameters and minimized along the sliding surface. It was found that the controller successfully achieved its task on both the SWT and using FAST.

5.2 Suggestions for Future Studies

One of the initial assumptions in this study was that the wind's behavior was perfectly known. However, in reality, there are inherent issues such as noise from the sensor and reading errors. For instance, when an anemometer is used to measure wind speed, the wind readings can be significantly affected by the presence of blade shadow. Moreover, while LIDAR can provide more accurate readings, it is a rather expensive solution to implement. Consequently, it is imperative that a properly developed estimator model is established to enhance the accuracy of the results.

In addition, other aspects such as tower displacement and blade bending were not initially considered in the study. If these factors were included, it is believed that the performance of the controller would be significantly improved. A suggestion for future research is to include pitch control in the wind turbine to transform the system into a multi-input one. Even though the inclusion of pitch control could potentially reduce the turbine's lifespan, it is likely to improve power generation.

Furthermore, both the reference tracker and the controller were tested on Simulink using the SWT and FAST models. To fully substantiate these results, it would be beneficial to conduct

tests using a real wind turbine. Implementation of the observer and controller in the field on a real turbine could help validate the simulation results.

The focus of this study was primarily on the Maximum Power Point Tracking (MPPT) control region of the wind turbine. However, future research could extend these results to all operating regions by incorporating blade pitch into the model. Moreover, considering a higher-order model of the wind turbine, which includes more degrees of freedom (DOFs), can be a valuable step for future control design. It is important to note that large wind turbines are flexible structures with many moving components. Therefore, the consideration of dynamic equations in the wind turbine model is crucial for designing optimal control.

References

[1] "Government of Canada legislates climate accountability with first net-zero emissions law," Jun. 30, 2021. https://www.canada.ca/en/environment-climate-change/news/2021/06/government-of-canada-legislates-climate-accountability-with-first-net-zero-emissions-law.html (accessed Dec. 20, 2021).

[2] A. Kumar, M. Z. U. Khan, B. Pandey, and S. Mekhilef, "Wind energy: a review paper," *Gyancity Journal of Engineering and Technology*, vol. 4, no. 2, pp. 29–37, 2018, doi: 10.21058/gjet.2018.42004.

[3] A. S. Darwish and R. Al-Dabbagh, "Wind energy state of the art: present and future technology advancements," *Renew. Energy Environ. Sustain.*, vol. 5, p. 7, 2020, doi: 10.1051/rees/2020003.

[4] U. kumar Nath and R. Sen, "A Comparative Review on Renewable Energy Application, Difficulties and Future Prospect," in *2021 Innovations in Energy Management and Renewable Resources(52042)*, Feb. 2021, pp. 1–5. doi: 10.1109/IEMRE52042.2021.9386520.

[5] M. Abdel-Halim, "Enhancing the Performance of Wind-Energy-Driven Double-Fed Induction Generators," *Qassim University Scientific Journal- Engineering and Computer Sciences*, vol. 7, pp. 23–42, Jan. 2014.

[6] M. O. L. Hansen, *Aerodynamics of wind turbines*, 2nd ed. London ; Sterling, VA: Earthscan, 2008.

[7] F. D. Bianchi, H. De Battista, and R. J. Mantz, *Wind turbine control systems: principles, modelling and gain scheduling design*. in Advances in industrial control. London: Springer, 2007.

[8] J. F. Manwell, J. G. McGowan, and A. L. Rogers, *Wind energy explained: theory, design and application*. John Wiley & Sons, 2010.

[9] A. Faizan, "Wind Turbine Blade Aerodynamics," *Electrical Academia*, Aug. 01, 2018. https://electricalacademia.com/renewable-energy/wind-turbine-blade-aerodynamics/ (accessed Jun. 04, 2023).

[10] "Wind Turbine Control Methods." https://www.ni.com/en/solutions/energy/condition-monitoring/wind-turbine-control-methods.html (accessed Jun. 04, 2023).

[11] A. Merabet, J. Thongam, and J. Gu, “Torque and pitch angle control for variable speed wind turbines in all operating regimes,” in *2011 10th International Conference on Environment and Electrical Engineering*, Rome, Italy: IEEE, May 2011, pp. 1–5. doi: 10.1109/EEEIC.2011.5874598.

[12] J. Chu, L. Yuan, Z. Chen, W. Xu, Z. Lin, and Y. Du, “A Torque Coordination Control Strategy for Wind Turbine Based on Pole Placement,” in *2018 37th Chinese Control Conference (CCC)*, Jul. 2018, pp. 7387–7393. doi: 10.23919/ChiCC.2018.8483512.

[13] B. Babu and S. Divya, “Comparative study of different types of generators used in wind turbine and reactive power compensation,” *IOSR Journal of Electrical and Electronics Engineering (IOSR-JEEE)*, pp. 2278–1676, 2017.

[14] S. Lang and E. McKeogh, “LIDAR and SODAR Measurements of Wind Speed and Direction in Upland Terrain for Wind Energy Purposes,” *Remote Sensing*, vol. 3, no. 9, pp. 1871–1901, Aug. 2011, doi: 10.3390/rs3091871.

[15] E. Simley, L. Pao, N. Kelley, B. Jonkman, and R. Frehlich, “Lidar wind speed measurements of evolving wind fields,” in *50th AIAA aerospace sciences meeting including the new horizons forum and aerospace exposition*, 2012, p. 656.

[16] J. M. Jonkman, M. L. Buhl, and others, *FAST user’s guide*, vol. 365. National Renewable Energy Laboratory Golden, CO, USA, 2005.

[17] Z. Ons, J. Aymen, and M. M. Nejib, “Extracting Maximum Power from Wind Turbines using Tip Speed Ratio, Hill- Climbing and Neural Network controllers,” *International Journal of Advanced Research in Electrical, Electronics and Instrumentation Engineering*, vol. 5, no. 12, p. 2016, 2016.

[18] A. S. Martyanov, A. O. Troickiy, and D. V. Korobatov, “Performance Assessment of Perturbation and Observation Algorithm for Wind Turbine,” in *2018 International Conference on Industrial Engineering, Applications and Manufacturing (ICIEAM)*, May 2018, pp. 1–5. doi: 10.1109/ICIEAM.2018.8728559.

[19] K. Shah, V. Gaur, S. Joshi, and N. Patel, “Maximum power point tracking methods for wind and solar conversion systems for standalone generation PSIM based perturb and observe method,” *International Journal of Engineering Research and Development (IJERD)*, pp. 46–54, 2015.

[20] R. M. Linus and P. Damodharan, “Maximum power point tracking method using a modified perturb and observe algorithm for grid connected wind energy conversion systems,” *IET Renewable Power Generation*, vol. 9, no. 6, pp. 682–689, 2015, doi: 10.1049/iet-rpg.2014.0070.

[21] K. N. Yu and C. K. Liao, “Applying novel fractional order incremental conductance algorithm to design and study the maximum power tracking of small wind power systems,” *Journal of applied research and technology*, vol. 13, no. 2, pp. 238–244, 2015.

[22] Y. Yang and E. Solomin, “Hill-Climbing Algorithm for the Wind Turbine Yaw System,” in *2021 International Ural Conference on Electrical Power Engineering (UralCon)*, Sep. 2021, pp. 561–565. doi: 10.1109/UralCon52005.2021.9559498.

[23] S. S. Kumar and P. Venkatesan, “Design and implementation wind power using hill climbing mppt algorithm,” *Middle-East journal of Scientific Research*, vol. 21, no. 1, pp. 80–87, 2016.

[24] N. Hure, “Model Predictive Control of a Wind Turbine”.

[25] F. Al-Obaidy, M. Abdulsada, and F. Abusief, “Speed control of wind turbine by using PID controller,” May 2009. doi: 10.13140/2.1.3717.5680.

[26] T. P. T. Slavov, “LQR power control of wind generator,” in *2018 Cybernetics & Informatics (K&I)*, Jan. 2018, pp. 1–6. doi: 10.1109/CYBERI.2018.8337530.

[27] A. Jess and R. Sharma, “Modelling, control and performance analysis of a 6 MW wind turbine,” in *2015 IEEE PES Asia-Pacific Power and Energy Engineering Conference (APPEEC)*, Nov. 2015, pp. 1–5. doi: 10.1109/APPEEC.2015.7381003.

[28] X. Yao, C. Guo, Z. Xing, Y. Li, and S. Liu, “Variable Speed Wind Turbine Maximum Power Extraction Based on Fuzzy Logic Control,” in *2009 International Conference on Intelligent Human-Machine Systems and Cybernetics*, Hangzhou, Zhejiang, China: IEEE, 2009, pp. 202–205. doi: 10.1109/IHMSC.2009.174.

[29] G. D. Skikos and A. V. Machias, “Design and Development of Fuzzy Logic Control Strategies for Wind Turbine Generators,” *Wind Engineering*, vol. 19, no. 5, pp. 235–248, 1995.

[30] Y. Shtessel, C. Edwards, L. Fridman, and A. Levant, *Sliding Mode Control and Observation*. in Control Engineering. New York, NY: Springer New York, 2014. doi: 10.1007/978-0-8176-4893-0.

[31] R. Ghazali, M. Rahmat, and A. Hashim, “Performance Comparison between Sliding Mode Control with PID Sliding Surface and PID Controller for an Electro-hydraulic Positioning System,” *International Journal on Advanced Science, Engineering and Information Technology*, vol. 1, Jan. 2011, doi: 10.18517/ijaseit.1.4.91.

[32] S. Zine, B. Mazari, M. A. Bouzid, and Y. Mihoub, “Sliding mode control of wind turbine emulator,” in *2014 International Renewable and Sustainable Energy Conference (IRSEC)*, Ouarzazate, Morocco: IEEE, Oct. 2014, pp. 822–826. doi: 10.1109/IRSEC.2014.7059902.

[33] E. Hossain, R. Perez, S. Padmanaban, F. Blaabjerg, and V. K. Ramachandaramurthy, “Sliding Mode Controller and Lyapunov Redesign Controller to Improve Microgrid Stability: A Comparative Analysis with CPL Power Variation,” *Energies*, vol. 10, pp. 1–24, Nov. 2017.

[34] D. Liu, Y. Xia, R. Li, and P. Liu, “Integral sliding mode control of low-speed wind turbine,” in *2019 chinese automation congress (CAC)*, 2019, pp. 605–609.

[35] A. Merabet, R. Beguenane, J. S. Thongam, and I. Hussein, “Adaptive sliding mode speed control for wind turbine systems,” in *IECON 2011 - 37th Annual Conference of the IEEE Industrial Electronics Society*, Nov. 2011, pp. 2461–2466. doi: 10.1109/IECON.2011.6119696.

[36] B. Beltran, T. Ahmed-Ali, and M. E. H. Benbouzid, “High-Order Sliding-Mode Control of Variable-Speed Wind Turbines,” *IEEE Transactions on Industrial Electronics*, vol. 56, no. 9, pp. 3314–3321, Sep. 2009, doi: 10.1109/TIE.2008.2006949.

[37] J. Pieper, “First order dynamic sliding mode control,” in *Proceedings of the 37th IEEE Conference on Decision and Control (Cat. No.98CH36171)*, Tampa, FL, USA: IEEE, 1998, pp. 2415–2420. doi: 10.1109/CDC.1998.757768.

[38] N. Padmanabhuni, “First Order Dynamic Sliding Mode Control of a Wind Turbine with Optimized Tip Speed Ratio,” *CDSR*, vol. 10, Jun. 2023, doi: 10.11159/cdsr23.217.

[39] E. Owen, “Unscented H-infinity Wind Speed Estimation and H-infinity Control of Wind Turbines,” PRISM, 2021. doi: 10.11575/PRISM/10182.

[40] A. Vahidi, A. Stefanopoulou, and H. Peng, “Recursive least squares with forgetting for online estimation of vehicle mass and road grade: theory and experiments,” *Vehicle System Dynamics*, vol. 43, no. 1, pp. 31–55, Jan. 2005, doi: 10.1080/00423110412331290446.

[41] C. Paleologu, J. Benesty, and S. Ciochina, “A Robust Variable Forgetting Factor Recursive Least-Squares Algorithm for System Identification,” *Signal Processing Letters, IEEE*, vol. 15, pp. 597–600, Feb. 2008, doi: 10.1109/LSP.2008.2001559.

[42] S. Spurgeon, “Sliding mode control: a tutorial,” in *2014 European Control Conference (ECC)*, Strasbourg, France: IEEE, Jun. 2014, pp. 2272–2277. doi: 10.1109/ECC.2014.6862622.

[43] C. M. Dorling and A. Zinober, “Hyperplane Design in Model-Following Variable Structure Control Systems,” *IFAC Proceedings Volume*, vol. 18, no. 5, pp. 1901--1905, 1985.

[44] G. F. Franklin, J. D. Powell, and A. Emami-Naeini, *Feedback control of dynamic systems*, Seventh edition. Boston: Pearson, 2015.

[45] M. N. Soltani, T. Knudsen, M. Svenstrup, and R. Wisniewski, “Estimation of Rotor Effective Wind Speed: A Comparison,” *IEEE Trans. Contr. Syst. Technol.*, vol. 21, no. 4, pp. 1155–1167, Jul. 2013, doi: 10.1109/TCST.2013.2260751.

[46] M. Carpintero-Renteria, D. Santos-Martin, A. Lent, and C. Ramos, “Wind turbine power coefficient models based on neural networks and polynomial fitting,” *IET Renewable Power Generation*, vol. 14, no. 11, pp. 1841–1849, 2020.

[47] J. Jonkman, S. Butterfield, W. Musial, and G. Scott, “Definition of a 5-MW Reference Wind Turbine for Offshore System Development,” NREL/TP-500-38060, 947422, Feb. 2009. doi: 10.2172/947422.

[48] B. J. Jonkman, “TurbSim user’s guide,” National Renewable Energy Lab.(NREL), Golden, CO (United States), 2006.